A search for auroral radio emission from exoplanets
太陽系外惑星のオーロラ電波の探査

by

Yuta Shiohira
潮平雄太

A Doctor Thesis
博士論文

Submitted to
Graduate School of Science and technology
of Kumamoto University
on March, 2024
in Fulfillment of the Requirements
for the Degree of Doctor of Philosophy

Supervisor: Keitaro Takahashi　高橋慶太郎

Contents

Chapter 1

Introduction

Since the first discovery of exoplanets by Wolszczan and Frail [1992], their number has increased rapidly with the development of technology (Fig. 1.1)[1]. This leads that it has become clear that not only they are planetary systems ubiquitous outside our solar system, but also that they have diverse properties that differ from the previous framework considered only for the solar system. This fact has brought us to the next stage of research, which is to characterise each exoplanet. One of the essential ways to characterise is to measure the strength of the exoplanetary magnetic field. This allows us to infer the properties and environment of exoplanets, such as the interior [e.g., Sánchez-Lavega, 2004, Reiners and Christensen, 2010, Lazio et al., 2019], the atmospheric escape [Zarka et al., 2015], the tilt of the magnetic axis with respect to the spin rotation axis [Hess and Zarka, 2011], and the plasma source flux. To detect the exoplanetary magnetic field, radio observation is expected to be one of the best methods.

In our solar system, Earth and giant planets have intrinsic magnetic fields generated

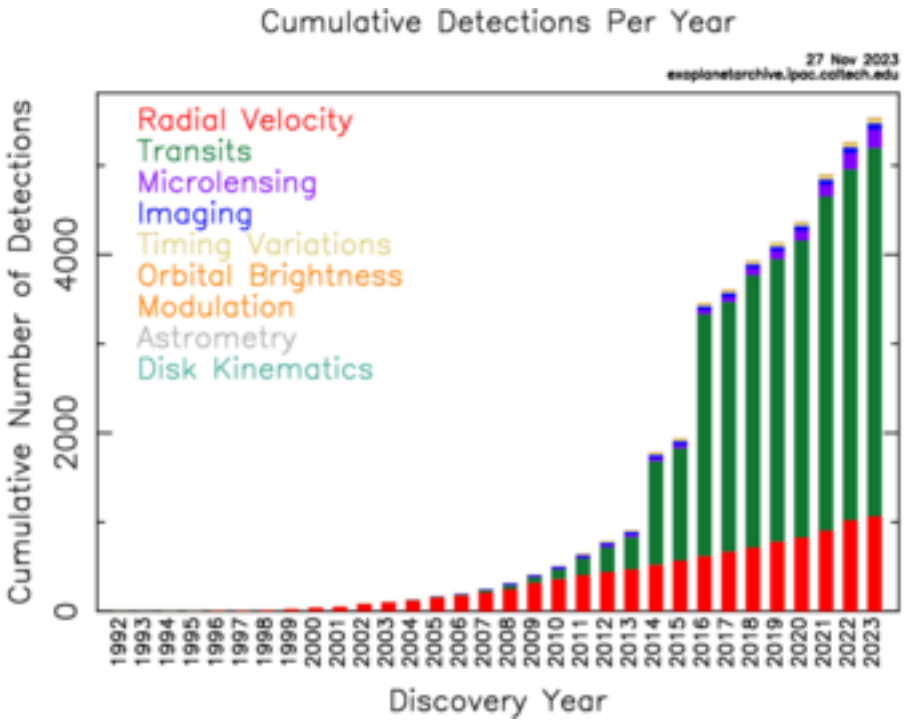

Figure 1.1: Cumlative number of detected exoplanets until 2023/11. So far, the colors show the detection method. 5,000 exoplanets have been detected. (Credit: NASA Exoplanet Archive)

[1] https://exoplanetarchive.ipac.caltech.edu/exoplanetplots

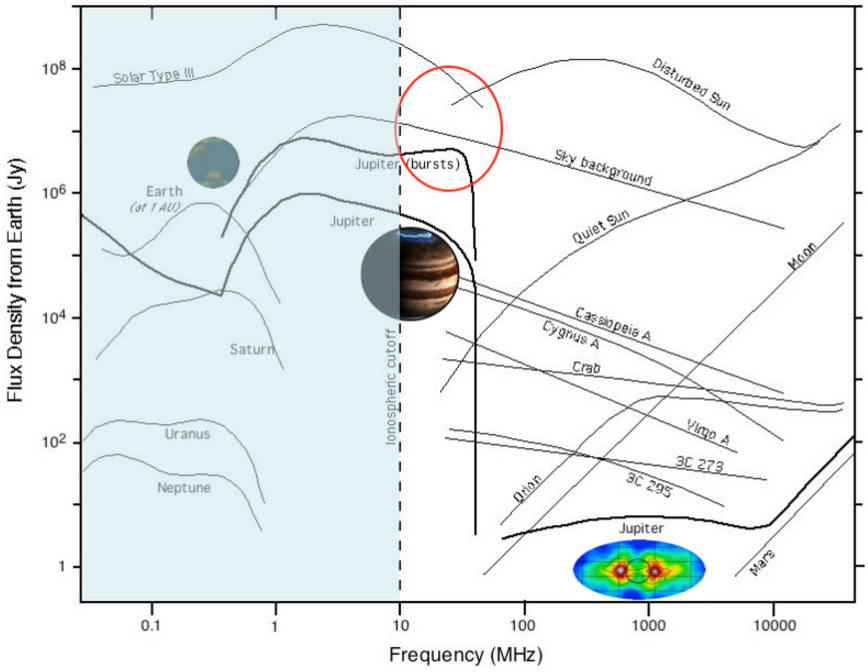

Figure 1.2: Spectra of detectable radio waves from the Earth [Zarka et al., 2015]. All spectra are considered the case they are observed from a distance of 1 AU. The red circle shows that the Jorvian radio emission from 10 to 40 MHz is close to the solar bursts. The shaded area displays an undetectable band because of the reflection by the Earth's ionosphere.

by the convective motions of conducting fluid inside the planets. By colliding with the solar wind, the space dominated by the planetary magnetic field, magnetosphere, is formed around the planets. The magnetosphere is the place where the interaction with the planetary magnetic field and the plasma supplied by such as the solar wind and moon and accelerated keV-MeV. These interactions generate less than a few tens of MHz radio emission, the auroral radio emission, via a coherent non-thermal mechanism, and the electron cyclotron maser instability (ECMI) [Wu and Lee, 1979, Zarka, 1998, Treumann, 2006]. For Jupiter, because it has the strongest magnetic field, ~10 G (at the polar region), the maximum frequency of the emission exceeds 10 MHz where is not reflected by the Earth's ionosphere, that is, it is detectable ground-based telescopes. Moreover, in contrast to the star-planet contrast at the optical and the infrared, which are 10^9 and 10^6, respectively, the emission is as intense as the sun at the low-frequency radio [Zarka et al., 2015] (Fig. 1.2). By analogy, we can infer from the magnetic planets in our solar system, especially Jovian auroral emission, that there would be magnetised exoplanets, and some of them have the potential to be intense radio sources. (On the other hand, remarkable, the existence of magnetized exoplanets and the detection of auroral emission from them have been envisioned since before the first detection of an exoplanet [e.g., Yantis et al., 1977, Winglee et al., 1986].)

After the discovery of exoplanets, the detected parameters of exoplanets, such as mass, radius and orbital parameters, allow us to estimate the flux of the auroral radio emission driven by various mechanisms by combining to the knowledge of the solar system planets. For the estimation of the power of auroral radio emission from exoplanets, it has been employed the scaling law so-called Radiometric Bode's law which is based on

the empirical proportional relation between the kinetic energy $P_{\rm kin}$ and magnetic energy $P_{\rm imf}$ of incident from the solar wind and the power of planetary radio emission $P_{\rm rad}$ (Fig. 1.3):

$$P_{\rm rad} = \alpha P_{\rm kin} = \alpha N m_p V^3 \pi R_{\rm MP}^2 \tag{1.1}$$

$$P_{\rm rad} = \beta P_{\rm imf} = \beta \left(B_\perp^2 / \mu_0 \right) V \pi R_{\rm MP}^2 \tag{1.2}$$

where N is the solar wind density, $m_{\rm p}$ is the mass of proton, V is the relative velocity of solar wind to the planetary motion, $R_{\rm MP}$ is the magnetopouse radius, $B_\perp$ is the interplanetary magnetic field perpendicular to the solar wind flow. α and β represent the energy conversion efficiencies and $\sim 10^{-5}$ and 2×10^{-3}, respectively. Considering the size of the magnetosphere and the properties of stellar wind control the flux of the auroral emission, it is preferred, as intense emitter, that exoplanets have strong magnetic fields and orbit around more active or nearby host stars. Thereby, in the case of hot Jupiter which is the massive planet orbiting nearby the host star, it is expected that it would be promising candidate if it has strong magnetic field. Zarka [2007] estimated the incident power of stellar wind would reach $10^3 - 10^5$ times larger than the Jupiter's one (Fig. 1.4), which indicates that hot Jupiter is still good target even considering the ram pressure and magnetic pressure of stellar wind compress the planetary magnetosphere. In addition, the advanced theories developing that idea have been proposed: interaction considering properties of the stellar wind, taking account of the actual observed data [Stevens, 2005], coronal mass ejection [Grießmeier et al., 2007], the dependence on the stellar age [Grießmeier et al., 2005, 2007], on the spectral type of the host star [Katarzyński et al., 2016], and the evolution after the main-sequence stars [Fujii et al., 2016].

The star-planet interaction scaled up Jupiter-Io system is also expected to be the mechanism driving the intense emission. In the Jupiter-Io system, the current formed by crossing Jupiter's magnetic field to Io's atmosphere composed of its volcanic activity connects the high latitude of Jupiter and Io, and the dissipated power in this system leads to the auroral emission [Thomas et al., 2004]. In the same way, the host star connected with close-in planets would also be the intense radio source. In this case of mechanism, auroral radio emission is radiated from the host star, not the planets.

Motivated by these theoretical studies, hot Jupiters and other planets that are likely to receive intense stellar wind are targeted by a number of observations, Ukrainian T-shaped Radio telescope, second modification (UTR-2) [Zarka et al., 1997, Ryabov et al., 2004, Zarka, 2011], Clark Lake Radio Observatory [Yantis et al., 1977], Green Bank Telescope (GBT) [Smith et al., 2009], Giant Metrewave Radio Telescope (GMRT) [Majid et al., 2006, Winterhalter et al., 2006, George and Stevens, 2007, Lecavelier Des Etangs et al., 2009, 2011, Lecavelier des Etangs et al., 2013, Hallinan et al., 2013, Narang et al., 2021a,b, Green and Madhusudhan, 2021], Low-Frequency Array (LOFAR) [Turner et al., 2017, O'Gorman et al., 2018, de Gasperin et al., 2020], Mizusawa [Shiratori et al., 2006], Muchison Widefield Array (MWA) [Murphy et al., 2015, Lynch et al., 2017, 2018], Very Large Array (VLA) [Bastian et al., 2000, Farrell et al., 2003, Lazio et al., 2004, Lazio and Farrell, 2007, Lazio et al., 2010a,b, Bower et al., 2016, Bastian et al., 2018], Very Long Baseline Array (VLBA) Bower et al. [2016], Westerbork Synthesis Radio Telescope (WSRT) [Stroe et al., 2012]. Although there is a recent claim of a tentative detection of a signal [Turner et al., 2021], no univocal detection has been made yet. Possible reasons include the observation frequency band being larger than the cut-off frequency of the auroral radio emission from the target, insufficient sensitivity and the emission beam did not direct to the Earth. For the reason of mismatch the frequency, because the maximum frequency $\nu_{\rm ce}$ of the auroral radio emission, is determined by the polar surface magnetic field strength $B_{\rm pol,p}$ of exoplanet,

$$\nu_{\rm ce} \sim 2.8\ {\rm MHz} \times B_{\rm pol,p}[{\rm G}], \tag{1.3}$$

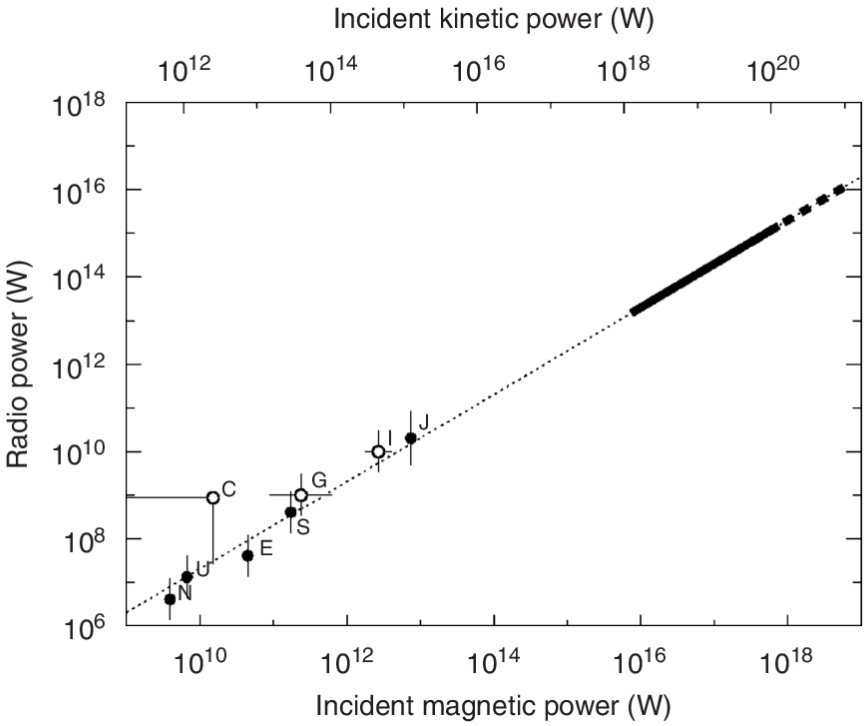

Figure 1.3: The scaling law of the intensity of the auroral radio emission (black doted line) [Zarka, 2007]. N, U, C, E, S, G, I, and J are taken from the initials of Neptune, Uranus, Callisto, Earth, Saturn, Ganymede, Io, and Jupiter, respectively. The x-axis shows the kinetic energy (upper side) and magnetic energy (lower side) of the solar wind to the planetary magnetic field, and the y-axis shows the intensity of emission from the objects. Note that, in the case of Galilean moons, the power dissipated by the input energy of plasma from Jupiter's magnetic field, instead of the solar wind, is displayed. The thick black solid line predicts the power of emission from hot Jupiter orbiting the sun-like star. A thick black dotted line also shows the power emission from the host star via star-planet interaction scaled up the Jupiter-Io system.

this cause would come from the weakness of the fields. According to Eq. 1.1 and Eq. 1.2, the magnetic field is an important parameter to determine the size of the magnetosphere, and hence, the weakness of the fields would leads also the planets to faint. On the other hand, some expectations of the flux [e.g., Griessmeier, 2017] indicates that the radio emission from several promising hot Jupiters would reach or exceed tens of mJy at low-frequency which has already been achieved by the above observations. Considering the solid angle of beam from Jupiter which is 1.6 sr and applying it to the beam from exoplanets, despite the ratio of beaming toward the earth being $1.6/(4\pi) \sim 0.13$ by considering simple geometry, it may be necessary to consider other factor to the flux estimation because no such intense hot Jupiters have yet been detected. So far, the following causes were suggested: expansion of the highly ionized upper atmospheres of hot Jupiters may hinder the generation of auroral emission due to the high local plasma frequency [Daley-Yates and Stevens, 2017, 2018, Weber et al., 2017a,b, 2018]. In addition, the fact that hot Jupiters are likely tidally locked to a synchronously rotating state might also suppress the emission by weakening the magnetic field strength [Grießmeier et al., 2004]. Overall, these considerations together with the no clear detection so far may indicate that the close-in planetary systems may not be as promising targets as initially thought.

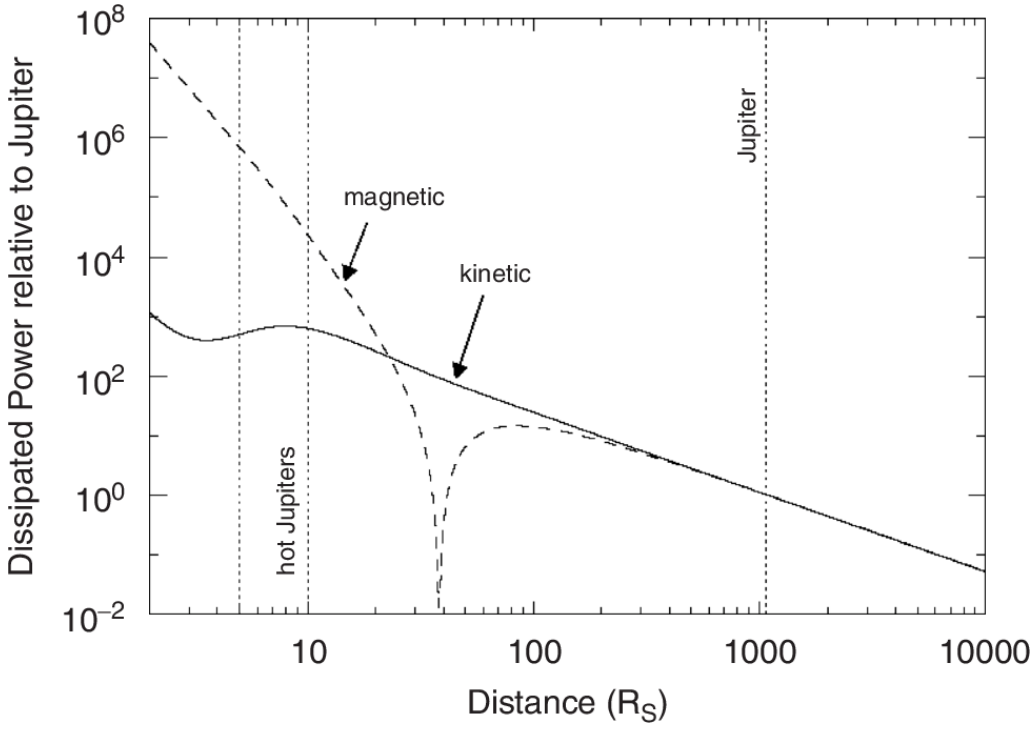

Figure 1.4: The dissipated stellar wind power (assuming host star as the sun) in magnetosphere of Jupiter and Jupiter-like hot Jupiter with semi-major axis shorter than 10 times solar radius [Zarka, 2007]. The horizontal axis is the deistance from the host star, and the vertical axis is dissipated power. The solid line and dashed line display the stellar wind's kinetic and magnetic power, respectively.

Taking into account the above, most of the previous theoretical and observational studies have focused on the direct detection of close-in exoplanets and have not yet led to a clear detection, we present two studies; one is an observation study targeting a long-orbit exoplanet, β Pic b, whose emission is induced by the interaction between the planetary magnetosphere and ionosphere, described in Chapter 2. Another is the new method for the detection by applying microlensing, described in Chapter 3.

Chapter 2

A search for radio emission from β Pic b

While the interaction with host stars is promising as a mechanism driving the detectable radio emission, the auroral emission may also be driven by the coupling between the magnetosphere and the ionosphere of the planet. A large fraction of Jovian auroral emission is powered by the current system connecting the magnetosphere and the ionosphere, which is driven by the interaction among Jovian planetary magnetic field ($\sim$ 10 G), the fast rotation ($\sim$ 10 h), and the plasma particles supplied by Io's volcanic activity [Hill, 1979]. By analogy, Nichols [2011, 2012] proposed that distant giant exoplanets with fast rotation, strong magnetic field and the supply of plasma into the magnetosphere would be suitable targets for radio observation. They also pointed out that the XUV intensity of the host star is also a key factor as high XUV irradiation onto the planet increases the ionospheric conductivity, resulting in a larger current. Exoplanets may also generate auroral emission by interacting with exomoons [Noyola et al., 2014, 2016]. Narang et al. [2023a] conducted the first search for signals from three exoplanets speculated to have Io-like exomoons with Giant Meterwave Radio Telescope (GMRT) and upgrade Giant Meterwave Radio Telescope (uGMRT). No signals were detected from the system on any exoplanetary systems, and the work put upper limits 0.18-1.6 mJy at 150, 325 and 400 MHz. In Narang et al. [2023b], another candidate which also may have volcanic exomoon was targeted by uGMRT observation. Still, the signals were undetected and put upper limits of 0.9-3.3 mJy at 150 MHz and 218 MHz.

These auroral emission mechanisms do not require the planet to be close to the host star. Exoplanets in distant orbits can also be a promising target of low-frequency radio observations.

Interestingly, auroral emission has been successfully detected from brown dwarfs [Berger et al., 2001, 2005, Berger, 2002, 2006, Berger et al., 2009, Burgasser and Putman, 2005, Burgasser et al., 2013, 2015, Osten et al., 2006, 2009, Hallinan et al., 2007, 2008, 2015, Phan-Bao et al., 2007, McLean et al., 2011, 2012, Antonova et al., 2013, Williams et al., 2013, Gizis et al., 2016, Lynch et al., 2016, Kao et al., 2016, 2018, Kao and Sebastian Pineda, 2022, Route and Wolszczan, 2016, Guirado et al., 2018, Richey-Yowell et al., 2020, Hughes et al., 2021, Climent et al., 2022, Vedantham et al., 2023] and recently from low-mass stars [Vedantham et al., 2020, Pérez-Torres et al., 2021, Callingham et al., 2021, Pineda and Villadsen, 2023]. Although the exact mechanism has not been elucidated, these emissions may be generated through the current system similar to that in the Jovian magnetosphere. Indeed, low-mass stars and brown dwarfs lie between Jovian planets and the solar-type stars in terms of mass and internal structure [Chabrier and Baraffe, 2000] and may develop similar magnetospheric structures. If they have a small companion, the system of the star (or brown dwarf) and the companion would be a scaled-up version of the Jupiter-Io system [e.g., Zarka, 2007, Saur et al., 2013, Turnpenney et al., 2018].

These observations also motivate one to search for the auroral emission from the young massive Jovian planets, as they have even more similarity to brown dwarfs in that

they have large heat flux from the interior and that they are more massive than Jupiter. According to one of the proposed scaling laws, these properties suggest the possibility of large magnetic field strengths of young Jovian planets (see Section 2.1 below). Large magnetic field strengths are also supported by the observations of gas accretion onto a young planet [Hasegawa et al., 2021].

Along this line, Cendes et al. [2022] conducted GHz frequency radio observations of five directly imaged young Jovian planets (Ross 458, GU Psc, 51 Eri, GJ 504 and HR 8799), with Very Large Array (VLA), and put upper limits at 6-210 μJy level. Narang [2022] analyzed observational data at frequencies from 150 MHz to 3 GHz obtained from GMRT and VLA to search for radio emission from the directly imaged exoplanet 1RXS1609 b and put upper limits 0.21-6 mJy. More survey is necessary to reveal the nature of the possible emissions from young Jupiter-like planets.

In this chapter, we present a search for the auroral radio emission in the 250-500 MHz bandpass from one of the best-studied exoplanets β Pictoris b. A unique aspect of this target among all the directly-imaged planets is its nearly edge-on orbit. It is known that the most vigorous Jupiter's auroral emission is observed from the equatorial plane due to the anisotropic nature of the radio emission [Ladreiter and Leblanc, 1989]. A similar anisotropy implies that the emission is highest if the planet is in an edge-on orbit, on the assumption that the obliquity of the planet (the angle between the orbital axis and the spin axis) is slight. β Pictoris b also has the measured rotation velocity, which suggests the rotation period of $\sim$ 8 hours [Snellen et al., 2014]. These factors would work favourably to observe the intense radio emission from this target.

The organization of this chapter is as follows: Section 2.1 presents the properties of β Pictoris b and the estimation of the maximum frequency and flux density of the emission. We describe observations and data analysis in Section 2.2 and report the results in Section 2.3. Lastly, we discuss the constraints on the β Pictoris b parameters in Section 2.4.

2.1 Target

The target planetary system in our observation is β Pictoris system, which is 19.75 pc away from the Earth. In this system, an A6 V star [Gray et al., 2006] hosts two exoplanets, β Pic b and c. Both of them are in long orbits and are massive (β Pic b: $a = 10.2^{+0.4}_{-0.3}$ AU, $M_{\rm p} = 12.8^{+5.3}_{-3.2}$ $M_{\rm J}$, β Pic c: $a = 2.68 \pm 0.02$ AU, $M_{\rm p} = 8.89 \pm 0.75$ $M_{\rm J}$ [Nielsen et al., 2020, Lacour et al., 2021]). This system is young, 22 Myr old [Mamajek and Bell, 2014], and the planet b has high effective temperature, $T_{\rm eff} = 1724 \pm 15$ K [Chilcote et al., 2017] due to the remnant accretion energy [Chilcote et al., 2017, Nowak et al., 2020].

The possible advantages of the systems in terms of the detectability of auroral radio emission are three-fold. First, according to the scaling law for the strength of the planetary magnetic field, planets which are massive and have high luminosity including β Pic b tend to have strong magnetic field. The maximum frequency of auroral emission is therefore expected to be high, potentially overlapping the GMRT bands with high sensitivity. Second, the rotation period of β Pic b is estimated to be $\sim$ 8 hr, based on the high-resolution spectra [Snellen et al., 2014], comparable to Jovian rotation period. The short rotation period would be necessary to drive strong auroral emission through magnetosphere-ionosphere (M-I) coupling similar to Jovian auroral emission. The estimated rotation period would also help us distinguish the auroral radio emission of the planet from other sources. Third, the planets have nearly edge-on orbit ($i = 88.88 \pm 0.09$ deg [Nielsen et al., 2020]). Jupiter's auroral radio emission is detectable only from near the equatorial plane due to the beaming effect [Ladreiter and Leblanc, 1989] (approximately ± 10 degree from the equator), and assuming the similar beaming and the small obliquity make planets on nearly edge-on orbits the only targets whose auroral emissions are detectable from Earth.

	Parameters	Values	Reference
System	Distance	19.75 pc	Gaia DR2 [Gaia Collaboration et al., 2016, 2018]
	RA	05h 47m 17.1s	
	Dec	−51° 03' 59"	
	Age	22 Myr	Mamajek and Bell [2014]
Host star	Spectral type	A6 V	Gray et al. [2006]
	Mass	1.77(± 0.03) $M_\odot$	Nielsen et al. [2020]
Planet (β Pic b)	Mass	$12.8^{+5.3}_{-3.2}$ M_J	Nielsen et al. [2020]
	Radius	1.46(±0.01) R_J	Chilcote et al. [2017]
	Effective temperature	1,724(±15) K	Chilcote et al. [2017]
	Semi-major axis	$10.2^{+0.4}_{-0.3}$ AU	Nielsen et al. [2020]
	Orbital period	$24.3^{+1.5}_{-1.0}$ yrs	Nielsen et al. [2020]
	Orbital inclination	88.88(±0.09) deg	Nielsen et al. [2020]
	Spin velocity	25(±3) km/s	Snellen et al. [2014]
	Spin period	8 hr (assuming zero obliquity)	

Table 2.1: The parameters for β Pic system, host star and β Pic b

These properties let us select β Pic b as the primary target of the search of the auroral radio emission from directly-imaged planets.

In the following, we describe how we estimate the frequency and flux density of the auroral radio emission of β Pic b.

2.1.1 Maximum frequency of radio emission

As described in Sec. 1, the maximum frequency $\nu_{\rm ce,max}$ of the auroral radio emission depends on the polar magnetic field $B_{\rm pol,p}$, given as Eq. 1.3. To predict the maximum frequency from that equation, it is necessary to estimate $B_{\rm pol,p}$. Several scaling laws for the strength of planetary magnetic field have been proposed so far. In this study, we consider the law of Christensen et al. [2009] and of magnetic Bode's law [e.g., Blackett, 1947, Russell, 1978, Farrell et al., 1999]. The main difference between the two is the dependence on the planetary rotation.

Christensen's scaling law states that the strength of the magnetic field on the surface of core region, $B_{\rm c,p}$, is independent of the planetary rotation and estimated by the following,

$$B_{\rm c,p}^2 \propto f_{\rm ohm}\rho_{\rm c,p}{}^{1/3}(Fq_{\rm o,p})^{2/3} \tag{2.1}$$

where $f_{\rm ohm}(\leq 1)$ is the ratio of the ohmic dissipation to the total dissipation, $\rho_{\rm c,p}$ is the mean density of the core, F is an efficiency factor and of order unity and $q_{\rm o,p}$ is the heat flux on the outer surface of the core. To estimate $B_{\rm c,p}$, it is necessary to evaluate $\rho_{\rm c,p}$ and $q_{\rm o,p}$.

To estimate the density profile within exoplanets where clues are virtually absent, it is helpful to employ the assumption of a polytropic gas sphere, $P = K\rho^{1+(1/n)}$, where P is Pressure, K is a constant, ρ is density and n is the polytropic index [e.g., Sánchez-Lavega, 2004, Grießmeier et al., 2007]. Here, we set the polytropic index $n = 1.5$ and numerically solved the Lane-Emden equation,

$$\frac{1}{\xi}\frac{d}{d\xi}\left(\xi^2\frac{d\theta}{d\xi}\right) = -\theta(\xi)^n, \tag{2.2}$$

where ξ and $\theta(\xi)$ are dimensionless radius and density, respectively, and they are defined using the radius r and density ρ of the sphere as follows:

$$\xi = \frac{r}{\alpha}\ ,\ \theta^n = \frac{\rho}{\rho_{\rm center}}, \tag{2.3}$$

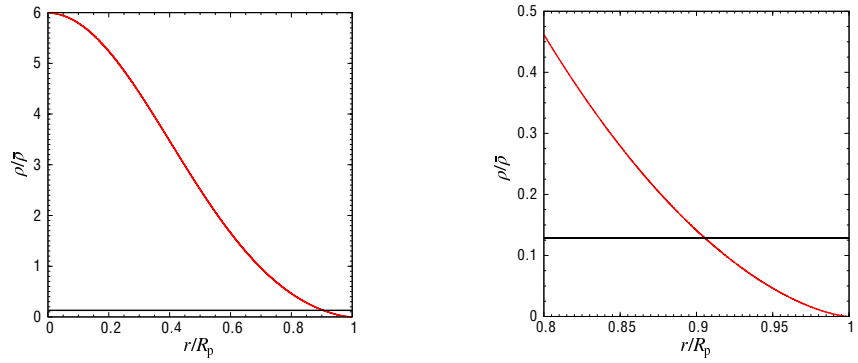

Figure 2.1: The estimation of the density profile of β Pic b. The vertical axis represents density, and the horizontal axis represents distance from the center. Each axis is normalized by the mean density and the radius of β Pic b, respectively. The red solid line shows the density profile. The black solid line corresponds to the density that hydrogen undergoes a phase transition to metallic, $\sim 0.7 \mathrm{g/cm^3}$. The right panel is an expanded version of the left panel.

where α is a constant, and ρ_{center} is the density at the center of sphere. Eq. 2.2 can be rewritten as two differential equations through the conversion $y_1 = \theta$ and $y_2 = \frac{d\theta}{d\xi} = \theta'$,

$$\begin{cases} \dfrac{dy_1}{d\xi} = y_2 \\ \dfrac{dy_2}{d\xi} = -\dfrac{2}{\xi} y_2 - y_1^n \end{cases}, \tag{2.4}$$

and we can then obtain the functions of θ and θ' by solving Eq. 2.4 with the initial conditions $\theta(0) = 1$ and $\theta'(0) = 0$. From the solutions, a mass M and a mean density $\bar{\rho}$ within an arbitrary distance r from the center can be determined:

$$M = \int_0^r 4\pi r^2 \rho(r) dr = -4\pi\alpha^3 \rho_{\mathrm{c}} \left(\xi^2 \frac{d\theta}{d\xi}\right). \tag{2.5}$$

$$\bar{\rho} = \frac{M}{\frac{4}{3}\pi r^3} = -\frac{3\rho_{\mathrm{c}}}{\xi}\left(\frac{d\theta}{d\xi}\right). \tag{2.6}$$

Then, the density normalized by the mean density of the entire sphere can be computed for each ξ applying the definition 2.3,

$$\frac{\rho}{\bar{\rho}} = \frac{\rho}{\rho_{\mathrm{center}}} \frac{\rho_{\mathrm{center}}}{\bar{\rho}} = -\frac{\xi\theta^n}{3}\left(\frac{d\theta}{d\xi}\right)^{-1}. \tag{2.7}$$

When each ξ is divided by $\xi = R/\alpha$, which is found by searching for the value of ξ such that $\theta = 0$, ξ also can be expressed in terms of the radius normalized by the sphere's radius r/R. Based on the above, we can estimate the density profile inside an arbitrary volume inside the radius r by substituting an object's parameters. For the $\beta Pic b$, Fig. 2.1 displays the estimated density profile. By determining the radius of the outer boundary of the core to be $r_{\mathrm{c,p}} \sim 0.9\ R_p$ based on the density that hydrogen undergoes a phase transition to metallic, $\sim 0.7\ \mathrm{g/cm^3}$[Grießmeier et al., 2007]. The core mass can computed by 2.5, therefore, we can estimate the core density, $\rho_{\mathrm{c,p}} \sim 7.254\ \mathrm{g/cm^3}$.

The $q_{\mathrm{o,p}}$ is estimated from the assumption that the luminosity of the planet is equal to the total energy flux at the surface of the core. Thus, denoting the effective temperature of the planet by $T_{\mathrm{eff,p}}$,

$$q_{\mathrm{o,p}} = \sigma_{\mathrm{sb}} T_{\mathrm{eff,p}}^4 \times \left(\frac{R_{\mathrm{p}}}{r_{\mathrm{c,p}}}\right)^2 \tag{2.8}$$

where $\sigma_{\rm sb} \sim 5.67 \times 10^{-8} {\rm Wm^{-2}K}$ is the Stefan-Boltzmann constant. We relate $B_{\rm pol,p}$ with $B_{\rm c,p}$ by

$$B_{\rm pol,p} \propto B_{\rm c,p} \left(\frac{r_{\rm c,p}}{R_{\rm p}}\right)^3 \propto {\rho_{\rm c,p}}^{1/6} {q_{\rm o,p}}^{1/3} \left(\frac{r_{\rm c,p}}{R_{\rm p}}\right)^3 \tag{2.9}$$

to find the scaling of the surface magnetic field strength as follows:

$$B_{\rm pol,p} = \left(\frac{\rho_{\rm c,p}}{\rho_{\rm c,J}}\right)^{1/6} \left(\frac{q_{\rm o,p}}{q_{\rm o,J}}\right)^{1/3} \left(\frac{r_{\rm c,p}}{r_{\rm c,J}}\right)^3 \left(\frac{R_{\rm J}}{R_{\rm p}}\right)^3 B_{\rm pol,J} \tag{2.10}$$

The subscript J indicates the Jovian values of the parameters: $\rho_{\rm c,J} \sim 1.899$ g/cm^3, $R_{\rm J} \sim 7.0 \times 10^7$ m, $r_{\rm c,J} \sim 0.85\ R_{\rm J}$, and $q_{\rm o,J} \sim 7.485 {\rm W/m^2}$ [Li et al., 2018]. Putting all the numbers above into Eq. 2.10 gives $B_{\rm pol,p} \sim 66\ B_{\rm pol,J}$. Therefore, the maximum frequency of auroral radio emission from β Pic b would be 66 times larger than that of Jupiter, about 1.8 GHz in this case.

Next, we estimate the frequency from the magnetic Bode's law, which suggests the proportionality between the angular momentum and magnetic moment of a planet:

$$B_{\rm eq,p} R_{\rm p}^3 \propto \omega_{\rm p} M_{\rm p} R_{\rm p}^2 \tag{2.11}$$

where $B_{\rm eq,J}$ is the surface magnetic field strength at the equator, and $\omega_{\rm p}$ ($\sim 1.25\ \omega_{\rm J}$) is the angular velocity of planetary rotation. Therefore, the surface magnetic field strength of β Pic b is expressed as follows,

$$B_{\rm pol,p} = \left(\frac{\omega_{\rm p}}{\omega_{\rm J}}\right) \left(\frac{M_{\rm p}}{M_{\rm J}}\right) \left(\frac{R_{\rm p}}{R_{\rm J}}\right)^{-1} \times B_{\rm pol,J} \tag{2.12}$$

where we assumed that the planetary magnetic field is a dipole field, that is $B_{\rm eq,J} = B_{\rm pol,J}/2$. The surface field strength at the polar of β Pic b is thus expected to reach $\sim 11\ B_{\rm pol,J}$. In this case, the maximum frequency is expected to be about 300 MHz.

In both cases, the maximum of the emission would be higher than 300 MHz and expected to be observable with uGMRT in band 3 (250-500 MHz).

2.1.2 Radio flux density

The main source of the auroral radio emission from β Pic b is considered to be the M-I coupling due to the fast rotation and the strong magnetic field estimated earlier. Assuming that the planetary magnetic field is a dipole field, the total power dissipated by the current system of M-I coupling, $P_{0,\rm J}$, is given by Hill [2001] as follows:

$$P_{0,\rm J} = \frac{2\pi \Sigma_{\rm J} B_{\rm eq,J}^2 \omega_{\rm J}^2 R_{\rm J}^4}{L_{\rm J}^2}, \tag{2.13}$$

where $\Sigma_{\rm J}$ is the height-integrated Pedersen conductivity in the polar ionosphere. $L_{\rm J}$ is the scale length representing the region in the equatorial plane of the planet where the magnetospheric plasma is co-rotating with the planet's rotation, and is given (in $R_{\rm J}$) as follows.

$$L_{\rm J} = \left(\frac{\pi \Sigma_{\rm J} B_{\rm eq,J}^2 R_{\rm J}^2}{\dot{M}_{\rm J}}\right)^{1/4} \tag{2.14}$$

where $\dot{M}_{\rm J}$ represents the plasma mass outflow rate. In the case of $\Sigma_{\rm J} \sim 0.6$ mho and $\dot{M}_{\rm J} \sim 2000$ kg/s, $L_{\rm J}$ is about 30 $R_{\rm J}$ [Hill, 2001]. In this study, we assume that the power

dissipated by the M-I coupling at β Pic b, $P_{0,\mathrm{P}}$ can be estimated by scaling each parameter of Eq. 2.13 and Eq. 2.14. From Eq. 2.14, the scale length for β Pic b, L_{p} is expressed by

$$L_{\mathrm{p}} = \left(\frac{\Sigma_{\mathrm{p}}}{\Sigma_{\mathrm{J}}}\right)^{1/4} \left(\frac{B_{\mathrm{eq,p}}}{B_{\mathrm{eq,J}}}\right)^{1/2} \left(\frac{R_{\mathrm{p}}}{R_{\mathrm{J}}}\right)^{1/2} \left(\frac{\dot{M}_{\mathrm{p}}}{\dot{M}_{\mathrm{J}}}\right)^{-1/4} L_{\mathrm{J}} \tag{2.15}$$

Thus, the total power dissipated by the current system of β Pic b's M-I coupling, $P_{0,\mathrm{P}}$ is expressed as follows.

$$P_{0,\mathrm{P}} = \left(\frac{\Sigma_{\mathrm{p}}}{\Sigma_{\mathrm{J}}}\right)^{1/2} \left(\frac{\omega_{\mathrm{p}}}{\omega_{\mathrm{J}}}\right)^{2} \left(\frac{R_{\mathrm{p}}}{R_{\mathrm{J}}}\right)^{3} \left(\frac{B_{\mathrm{eq,p}}}{B_{\mathrm{eq,J}}}\right) \left(\frac{\dot{M}_{\mathrm{p}}}{\dot{M}_{\mathrm{J}}}\right)^{1/2} P_{0,\mathrm{J}} \tag{2.16}$$

Both Σ_{p} and $\dot{M}_{\mathrm{p}}$ are uncertain. The conductivity would depend on the EUV flux that the planet receives. Taking account of the semi-major axis of β Pic b and the EUV flux of β Pic b approximately 1 order of magnitude smaller Sanz-Forcada et al. [2011], the conductivity may be estimated to be $\Sigma_p = (5.2/10.2)^2\ (1/10)\ \Sigma_J \sim 0.03\ \Sigma_J$. Assuming $\dot{M}_{\mathrm{p}} = \dot{M}_{\mathrm{J}}$ and $B_{\mathrm{eq,P}} = 66\ B_{\mathrm{eq,J}}$, the total dissipated power $P_{0,\mathrm{p}}$ would be $\sim 53\ P_{0,\mathrm{J}}$. Assuming further that the ratio of the power of auroral radio emission to the total dissipated power is the same as Jupiter ($\sim 10^{-3}$; Zarka [2007]), the power of the auroral radio emission from β Pic b, $P_{\mathrm{rad,p}}$ would be expected to be 3.3×10^{13} W, where we adopted the nominal value of the total power dissipated in the Jovian M-I coupling, $P_{0,\mathrm{J}} = 6.0 \times 10^{14}$ W [Hill, 2001].

The flux density of auroral radio emission S_{p} is calculated using $P_{\mathrm{rad,p}}$, solid angle Ω, bandwidth of the emission $\Delta\nu$, and distance d from the earth to β Pic system:

$$S_{\mathrm{p}} = \frac{P_{\mathrm{rad,p}}}{\Omega d^2 \Delta\nu}. \tag{2.17}$$

Assuming that the bandwidth of the auroral radio emission is half of the maximum frequency following e.g., Farrell et al. [1999], that the solid angle of the beam is the same as Jupiter's, and $d = 19.75$pc, the estimated the auroral radio emission's flux density is $S_{\mathrm{p}} \sim 6.0\ \mu$Jy.

Ashtari et al. [2022] also estimated the flux density from β Pic b and c, driven by stellar wind-planet interaction. They predicted it would reach tens to hundreds of uJy, more than ten times our estimate. The gap comes because the maximum emission frequency is a difference of two orders of magnitude while the power of auroral radio emission is almost the same or differs by only several times less than the prediction of Ashtari et al. [2022]. We attribute the discrepancy in the flux density to the assessment of the strength of the planetary magnetic field, especially $q_{\mathrm{o,p}}$. Ashtari et al. [2022] employed two scaling laws proposed by Stevenson [1983] and Mizutani et al. [1992] for estimating the planetary magnetic moment; the magnetic moment is scaled by $\rho_{\mathrm{c,p}}^{1/2} r_{\mathrm{c}}^{3-3.5}$ in the case of beta Pic b and c because the angular velocity of rotation period and the core conductivity have been assumed same as Jupiter. Compared to our computations, the values of $\rho_{\mathrm{c,p}}$ and r_{c} are almost the same as the estimation in Sec. 2.1.1, and these terms make only several times the difference between scaling laws. On the other hand, $q_{\mathrm{o,p}}$ in Eq. 2.10 becomes larger as the object temperature is higher. In the case of β Pic system as a young system, since the planet's effective temperature is high, $T_{\mathrm{eff,p}} > 10^3$K, $q_{\mathrm{o,p}}$ contributes about 50 times larger than Jupiter to the magnetic moment. Therefore, the estimate of magnetic field strength by Christensen et al. [2009] used in Sec. 2.1.1 tends to be stronger for high-luminosity planets than the estimates based on the scaling laws of Stevenson [1983] and Mizutani et al. [1992] used in Ashtari et al. [2022], resulting in the differences in flux density described above. Note that in estimating flux density, the estimates can easily be changed by assumptions on uncertain parameters such as $\rho_{\mathrm{c,p}}$ and $q_{\mathrm{o,p}}$.

Date	On source time (hr)	Synthesized beam size (arcsec×arcsec)	rms noise (μJy beam^{-1})
2020 Jun 19	2.3	13.4×4.5	121
2020 Jul 11	2.0	16.6×4.3	88
2020 Sep 01	1.9	15.0×4.8	82
2020 Sep 16	1.5	16.0×4.9	94
(Stacking all)	7.7	14.5×4.7	60

Table 2.2: Summary of the observations and images.

2.2 Observation and data analysis

We observed the β Pic system with the uGMRT on 19 June, 11 July, 1 September and 16 September 2020. About 2 hours of observation were carried out at band 3 (centered at 400 MHz with a bandwidh of 200 MHz) each day. On every observation day, we conducted the following routine: First, we observed 3C147 for 10 min as a flux and bandpass calibrator. After that, J0538-440, the phase calibrator, and β Pic were observed for 5 min and about 30 min, respectively and alternately. In the last 10 min, 3C147 was observed again.

For the reduction of data, we used the pipeline that is CAsa Pipeline-cum-Toolkit for Upgraded Giant Metrewave Radio Telescope data REduction(CAPTURE) [Kale and Ishwara-Chandra, 2021]. It executes tasks, flagging, calibration, imaging and self-calibration utilizing Common Astronomy Software Applications (CASA).

In the first step, raw visibility data was flagged using CASA tasks `flagdata`. The frequency channel 0 and first and last 10 s of each scan were flagged. After that, calibration for delay, bandpass and gain were carried out. Flagging and calibration performed again. After this procedure, we use CASA's `tclean` task for imaging. The size of pixel in these images are $1.0'' \times 1.0''$. After imaging, 4 rounds of phase only self-calibration and 4 rounds of phase and amplitude self-calibration were executed. For final images made through the pipeline, we carried out primary beam correction with tasks `wbpbgmrt`[1].

2.3 Results

We detect no radio emission from β Pic b and set $3\sigma_{\rm rms}$ upper limit for each of four observations.

Fig. 2.2 shows the radio flux contours with the overlaid gray-scale image made by 2MASS All-Sky Data Release at J-band which can be obtained from *Interactive 2MASS Image Service* [2], and the location of the β Pic is marked with a red dot in each image. We computed the root-mean-square (rms) noise of each image on the area where $150'' \times 150''$ centerd the target, surrounded by red solid line on the image. The results are listed on Table 2.2, and the contours on Fig.2.2 indicate 5,10,15,20 times rms noise.

The rms noise is substantially larger than the nominal value of band 3 ($\sim$ 11.5 μJy). This is likely due to the low-elevation of the observations. When observing an object at low-elevation with interferometre, projected baselines are shortened, and the beam was stretched in Declination direction about two time than the ideal size [Gupta et al., 2017]. This beam expansion would lead to increase the noise level.

In addition, our observation was affected by the side-lobe of intense radio sources which locate near the target. Fig. 2.3 shows the zoom-out of Fig. 2.2, where the contours

[1] https://github.com/ruta-k/uGMRTprimarybeam
[2] https://irsa.ipac.caltech.edu/applications/2MASS/IM/interactive.html

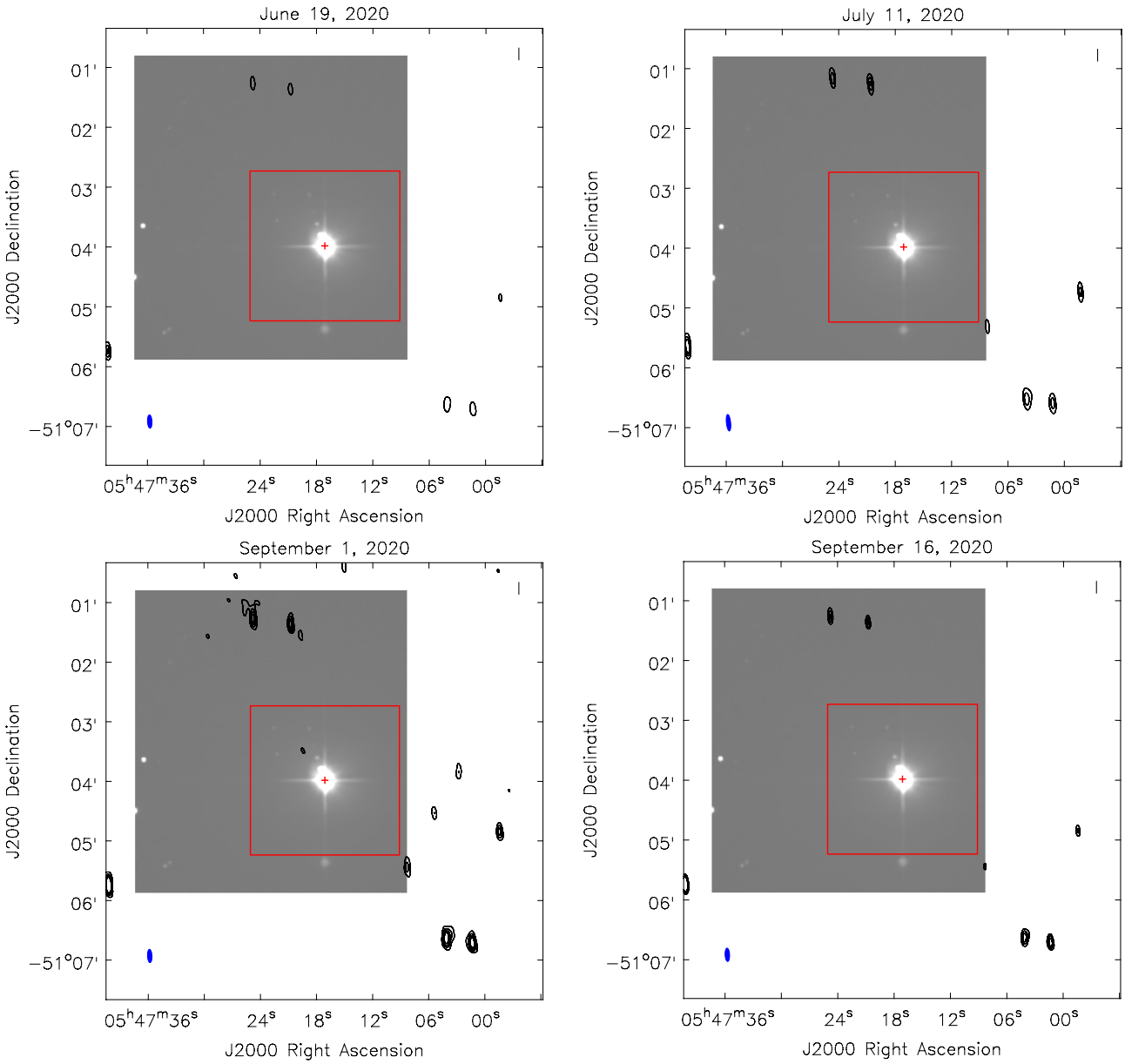

Figure 2.2: The uGMRT image for each of the four observation day expressed in contours. All are overlaid on 2MASS infrared image. Contours are set to 5,10,15,20 $\times\sigma_{\rm rms}$, where $\sigma_{\rm rms}$ are computed in the area surrounded red solid line, $150'' \times 150''$, and $\sigma_{\rm rms}$ = 121 μJy (6/19), 88 μJy (7/11), 82 μJy (9/1), 94 μJy (9/16). The red cross displays the position of the β Pic. The blue ellipse shown at left corner express the beam size.

are now 5, 10, 15 and 20 times the 60 μJy. Clearly visible two sources that extend to the position of the target are most likely J054806.4-505206(RA = 05h48m7s, Dec = $-50°52'7''$) and J054637.6-504830(RA = 05h46m38s, Dec $-$ $50°48'28''$) with flux densities of about 0.1 Jy and 0.2 Jy, respectively. While the mrs noise of the background is ~60 μJy, that in the side-lobe including the position of our target is more than 80 μJy.

We made a deeper image combining all four observations, shown in Fig. 2.4, and calculated the rms noise in the same way as Fig. 2.2 to find 60 μJy. This value was 10 times lager than the predicted value of flux density, and no signal was also detected. Then, we set the upper limit of $3\sigma_{\rm rms}$ = 180 μJy.

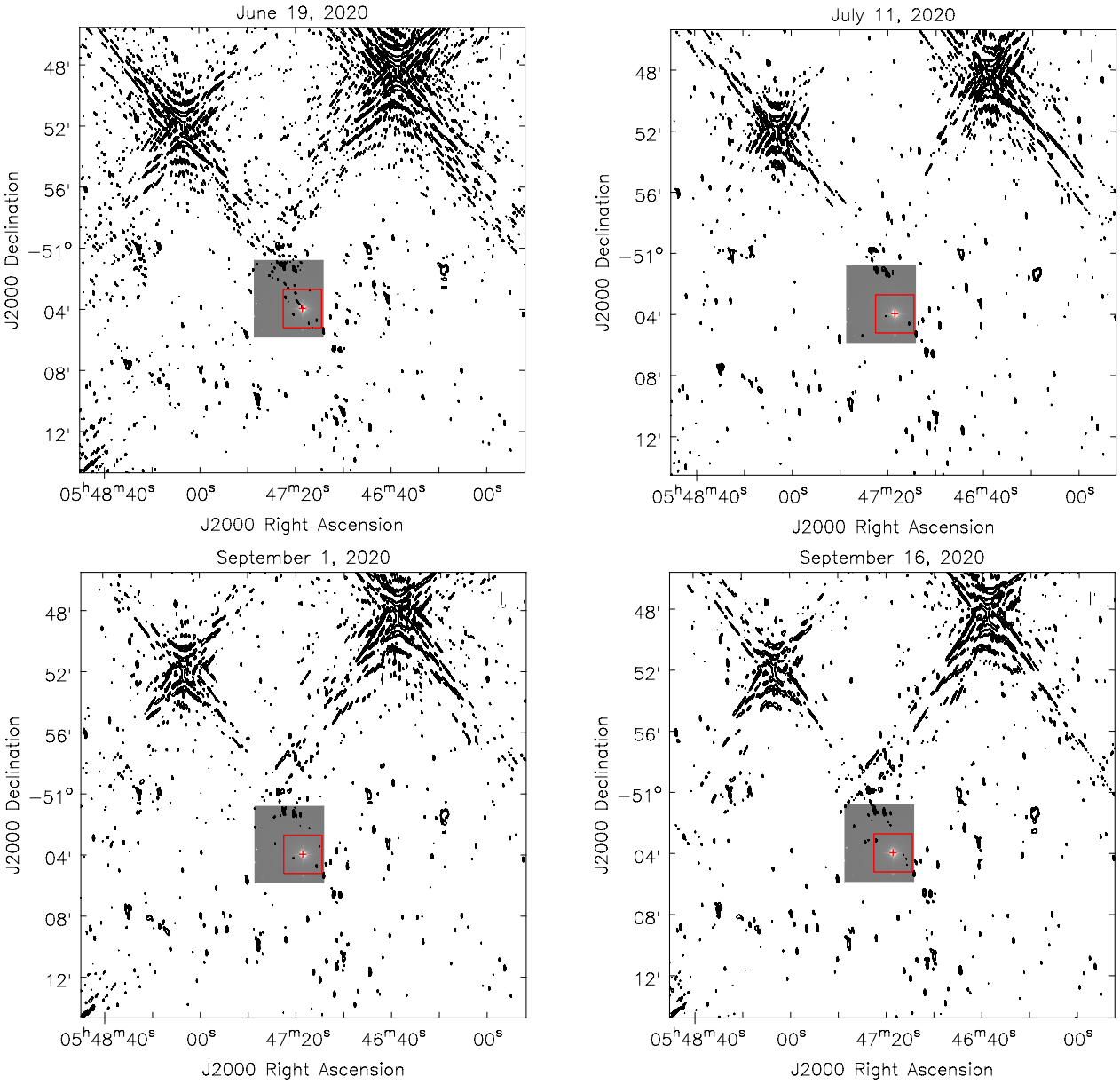

Figure 2.3: The uGMRT image for each of the four observation day expressed in contours. Contours are plotted 5,10,15,20 × 60 μJy which value is the quietest rms noise level in the field of view. The red square located near the center of the image is same area as shown in Fig. 2.2. The red cross displays the position of the β Pic.

2.4 Discussion

In this study, we have reported the results of the observation of the auroral radio emission from β Pic b using uGMRT with band 3. We estimated that it could generate a strong magnetic field and intense auroral radio emission through a mechanism similar to Juptier. However, we could not find any signals from the β Pic system and put the 3σ upper limit of ~ 180 μJy.

While this upper limit is larger than our nominal estimate of the radio emission, we could translate this limit to the constraints on the combination of the planetary parameters, assuming that the planetary radio emission arrives at Earth but was not detected due only to the insufficient sensitivity. Let us first consider the case where the planetary magnetic

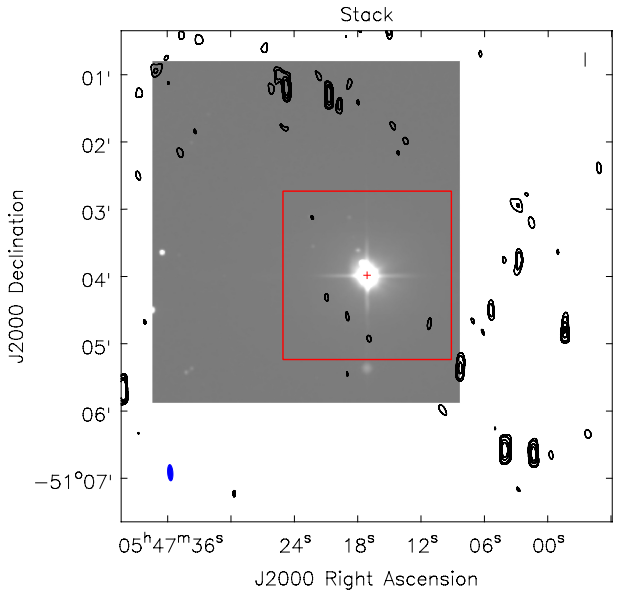

Figure 2.4: The deep image made by combining the visibility data obtained from all four observations, which is overlaid on 2MASS infrared image. Contours are set to 3,5,10,15 $\times\sigma_{\rm rms}$, where $\sigma_{\rm rms}$ are also computed in the area surrounded red solid line, $150'' \times 150''$, and $\sigma_{\rm rms} = 60$ μJy. The red cross displays the position of the β Pic. The blue ellipse shown at left corner express the beam size.

field is stronger than 10 $B_{\rm pol,J}$, i.e., the maximum frequency of the emission is within or larger than the bandpass of band 3 of uGMRT. Based on the scaling laws introduced in Sec. 2, the emission flux density is given by

$$S_{\rm p} = \frac{\left(\frac{\omega_{\rm p}}{\omega_{\rm J}}\right)^2 \left(\frac{R_{\rm p}}{R_{\rm J}}\right)^3 \alpha_{\rm J} P_{0,\rm J}}{\Omega d^2 (2.8\times10^6 \times B_{\rm pol,J}[\rm G])} \times \frac{\alpha_{\rm p}}{\alpha_{\rm J}} \left(\frac{\Sigma_{\rm p}\dot{M}_{\rm p}}{\Sigma_{\rm J}\dot{M}_{\rm J}}\right)^{1/2} \tag{2.18}$$

where α is the efficiency of the dissipation power to the emission power ($\alpha_{\rm J} \sim 10^{-3}$). To apply the upper limit, which was derived from the rms noise of the deepest image, to the parameter constraints, we should consider the total duration of the beam illuminating the Earth $\Delta t'$ and the emission bandwidth occupied within the bandpass $\Delta\nu'$. The upper limit modified for parameter constraints is thus given by

$$S_{\rm p,lim} = 180[\mu{\rm Jy}] \times \left(\frac{\Delta t'}{7.7{\rm hr}}\right)^{-1/2} \left(\frac{\Delta\nu'}{200{\rm MHz}}\right)^{-1/2} . \tag{2.19}$$

In this paper, we determined $\Delta t'$ by combining the parameters, rotation period $T_{\rm rot}$, the beam solid angle Ω and initial phase of beam ϕ. The strength of planetary surface magnetic field controls and $\Delta\nu'$. Substituting $S_{\rm p}$ in Eq. 2.18 by $S_{\rm p,lim}$, we obtained the upper limit of the product of α, $\Sigma_{\rm p}$ and $\dot{M}_{\rm p}$.

If the maximum frequency of the emission is within the bandpass of band 3 (between 250 MHz and 500 MHz), the radio flux detectable in band 3 is reduced and the constraints on the combination of these parameters are weakened accordingly. On the other hand, if the maximum frequency is below the observation bandpass, the only constraint may be put on the magnetic field strength. The constraints based on these considerations are summarized in Fig. 2.5 where the region filled with the diagonal lines are allowed.

We note that there remains the possibility that the emission is not directed toward the Earth. This possibility includes not only the case where the beam is always away from

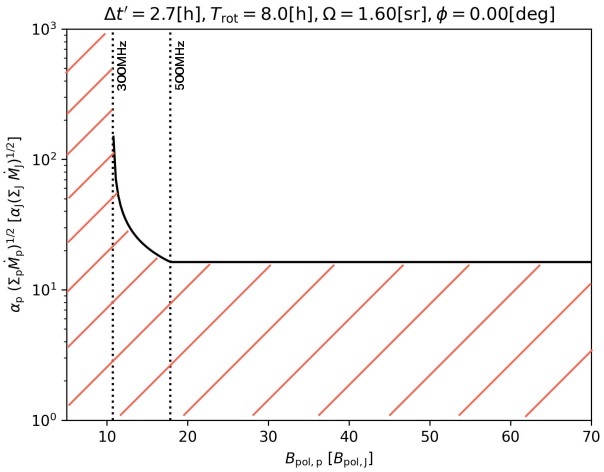

Figure 2.5: The most strict upper limit of the product of $\alpha_{\rm p}$, $\Sigma_{\rm p}$, and $\dot{M}$p for each magnetic field is derived with the longest observable time $\Delta t' = 2.7$h. The range of the product is restricted red shaded area. Two dotted lines illustrate the magnetic field strength which correspond to boundaries of bandwidth, 300 MHz and 500 MHz.

the Earth but also the case where the beam happened to be away from the Earth in all of the observation periods. If the former is the case, it implies that the obliquity of the planet is larger than Jupiter, or the tilt of the magnetic field is substantial, both of which provide constraints on the formation of Jupiter-like planets.

In either case, this system would be one of the important targets in the observations with Square Kilometre Array (SKA), which will cover the frequency range similar to our observations with higher sensitivity. Because it is located in the Southern hemisphere, it can continuously monitor the target for a longer time and would be less affected by the side-lobes we found, and it will provide a tighter constraint on the combination of planetary parameters to the level of our nominal estimate.

Chapter 3

Microlensed Radio Emission from Exoplanets

As mentioned in Sec. 1, no clear detection of the auroral radio emission from exoplanets has been reported. However, detecting it may be only matter of time. the upgrade to the existing observatories [e.g., GMRT] or the new capabilities [e.g., NenuFAR] are facilitating the more sensitive search toward the first univocal detection. Furthermore, the planned Square Kilometer Array (SKA) will conduct a sensitive survey at this frequency domain, and will provide the number of candidates. Motivated by these developments toward searching for exoplanetary auroral emission, we study the exoplanetary auroral emission observed through gravitational microlensing. We consider the scenario in which the planetary system with a hot Jupiter is the *source* of the lensing event[1]and the planetary auroral emission dominates the light from the source system at the considered wavelength/frequency (for microlensing event of radio emission from extra-terrestrial intelligence, see Rahvar [2016]). In general, gravitational microlensing amplifies the light from the source and allows us to detect the signal at a larger distance, typically closer to the Galactic Center where the occurrence rate of gravitational microlensing is high. Therefore, using microlensing, we can in principle study the magnetic properties of exoplanets at locations different from many known exoplanets.

The condition that the emission predominantly comes from the planet, the lighter body in the system, causes a notable difference from the microlensing magnification of the planetary system in the optical or infrared domains [Graff and Gaudi, 2000, Sajadian and Rahvar, 2010, Bagheri et al., 2019]. Because the source orbits the star with the period of $O(1)$ days, much shorter than the typical timescale of magnification, the magnification curve has a characteristic wavy feature depending on the orbital parameters. This would allow us to identify the planetary nature of the emission, and constrain some of the orbital parameters as well as the properties of the radio emission. We discuss these characteristic patterns in the magnification curve and evaluate the occurrence probability of such events.

The organization of this paper is as follows. In section 3.1, we introduce the framework of gravitational microlensing of an exoplanet as a source. Next, we show magnification curves and consider the relation between their feature and parameters of the system in section 3.2. In section 3.3, we discuss the observability of distant hot Jupiters through microlensing. Section 3.4 is devoted to discussion.

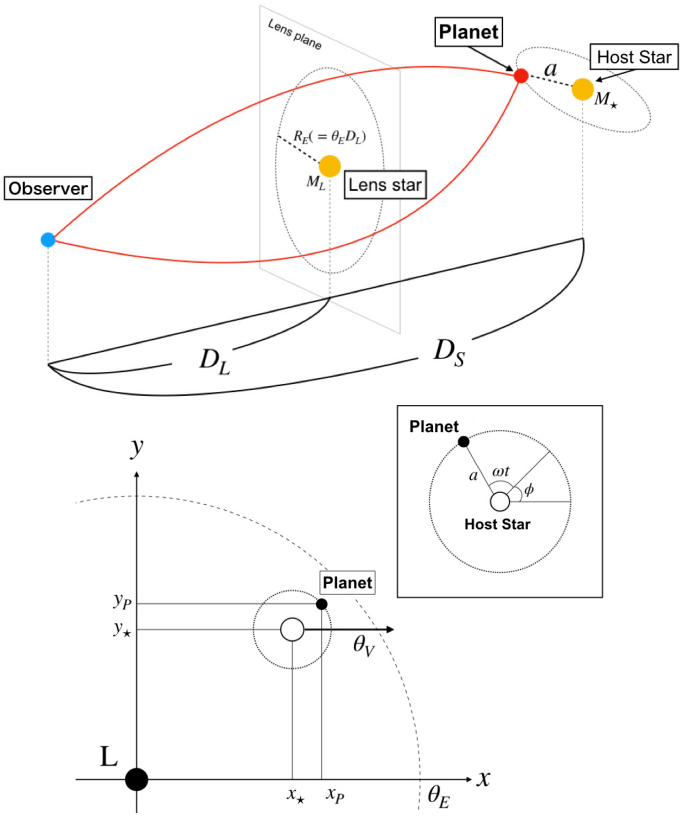

Figure 3.1: Schematic view of the configuration considered in this paper (top) and the coordinates on the lens plane (bottom). In the left panel, M_L and $M_\star$ are the masses of the lens star and host star, respectively, and D_L and D_S are the distance from the observer to the lens star and source star, respectively. In the right panel, the lens star is located at the origin on the lens plane. The position of the host star and planet are designated as $(x_\star, y_\star)$ and (x_P, y_P), respectively. θ_V is the relative transverse speed of lens and host star on the lens plane, a, ω and ϕ are the semi-major axis, angular velocity and initial orbital phase of the planet, respectively.

3.1 Microlensing of exoplanets

3.1.1 Gravitational lensing by a single star

Here we present a basic formalism to study microlensing of an exoplanet orbiting around the host star. The configuration we are considering is depicted in Fig. 3.1. First, the Einstein radius, θ_E, is defined as,

$$\begin{aligned}\theta_E &\equiv \sqrt{\frac{4GM_L}{c^2}\frac{D_S - D_L}{D_S D_L}} \\ &\sim 0.001\ [\mathrm{arcsec}] \left(\frac{M_L}{M_\odot}\right)^{\frac{1}{2}} \left(\frac{7[\mathrm{kpc}]}{D_S}\right)^{\frac{1}{2}} \left(\frac{D_S - D_L}{D_L}\right)^{\frac{1}{2}} , \end{aligned} \tag{3.1}$$

where M_L is the lens mass, D_L and D_S are the distance from the observer to the lens and source, respectively. When the host star passes through the Einstein ring, the rate at

[1]This is in contrast to the conventional microlensing method to discover exoplanets in which exoplanets are with the *lens* stars.

which the angular distance between the lens and the host star changes is given by

$$\begin{aligned}\dot{\theta} &= \frac{V}{D_L} \\ &= 0.012\ [\mathrm{arcsec/yr}] \left(\frac{V}{200\ [\mathrm{km/s}]}\right)\left(\frac{3.5[\mathrm{kpc}]}{D_L}\right) \end{aligned} \tag{3.2}$$

where V is the relative transverse speed of the lens and host star on the lens plane. The crossing time t_E, a characteristic timescale for the host star to cross the Einstein ring, is given as

$$\begin{aligned} t_E &= \frac{\theta_E}{\dot{\theta}} \\ &\sim 0.26\ [\mathrm{yr}] \left(\frac{M_L}{M_\odot}\right)^{\frac{1}{2}} \left(\frac{D_L}{3.5\ [\mathrm{kpc}]}\right)^{\frac{1}{2}} \left(\frac{D_S - D_L}{D_S}\right)^{\frac{1}{2}} \\ &\quad \times \left(\frac{100\ [\mathrm{km/s}]}{V}\right). \end{aligned} \tag{3.3}$$

The magnification A due to microlensing, is given by,

$$A = \frac{2+u^2}{u\sqrt{u^2+4}} \tag{3.4}$$

where $u = \theta_S/\theta_E$ and θ_S is the angular distance between the lens and source (planet). We denote the minimum angular distance between the lens and host star (rather than the planet) divided by the Einstein radius as u_{min}.

As shown in the right panel of Fig. 3.1, we assume that the host star moves in the x direction on the lens plane and the motion is expressed as $(x_\star, y_\star) = (\theta_V t, y_\star)$. Then, the motion of the planet (source) around the host star projected on the lens plane is expressed as,

$$\begin{pmatrix} x \\ y \end{pmatrix} = \begin{pmatrix} x_\star \\ y_\star \end{pmatrix} + \frac{a}{D_S} \begin{pmatrix} \cos\Omega & -\sin\Omega\cos i \\ \sin\Omega & \cos\Omega\cos i \end{pmatrix} \begin{pmatrix} \cos(\omega t + \phi) \\ \sin(\omega t + \phi) \end{pmatrix}, \tag{3.5}$$

where a is the semi-major axis, ω is the angular velocity of orbital motion, ϕ is the initial orbital phase of the planet, i is the orbital inclination and Ω is longitude of the ascending node. Here we assume a circular orbit for simplicity. Thus, the current system is characterized by 10 parameters: $M_\star$, M_L, D_S, D_L, a, u_{min}, V, ϕ, i and Ω. By substituting Eqs. (3.5) into Eq. (3.4), we can calculate the evolution of magnification of the planet. Finally, it is instructive to see the angular scale of the semi-major axis divided by the Einstein radius,

$$\begin{aligned} u_{\mathrm{a}} &\equiv \frac{a/D_S}{\theta_E} \\ &= 1.5\times10^{-2} \left(\frac{a}{0.1\ \mathrm{AU}}\right)\left(\frac{M_L}{M_\odot}\right)^{-\frac{1}{2}} \left(\frac{D_S}{7\ \mathrm{kpc}}\right)^{-\frac{1}{2}} \left(\frac{D_L}{D_S - D_L}\right)^{\frac{1}{2}}. \end{aligned} \tag{3.6}$$

3.2 Magnification curve

In this section, we show the magnification curves of microlensed exoplanets calculated from the formulation given in the previous section. Here, it should be noted that we are

Parameters	Values
$M_\star$	$M_\star = 1.0 M_\odot$
M_L	$M_L = 0.1 M_\odot, 1.0 M_\odot$
D_S	
D_L	
a	$R_\odot \leq a \leq 0.1$AU
$u_{\rm min}$	$0 \leq u_{\rm min} \leq 1$
V	
ϕ	$0^\circ \leq \phi \leq 360^\circ$
i	$0^\circ \leq i \leq 180^\circ$
Ω	$0^\circ \leq \Omega \leq 180^\circ$

Table 3.1: Parameters and their values.

considering a case where the planet is intrinsically much brighter than the host star so that only the planet can be observed even in the presence of microlensing if the magnifications are comparable.

Fig. 3.2 shows an example trajectory and magnification curve of a microlensing event of a planet with a small semi-major axis, $a = 0.1$ AU. Here, other parameters are set as $M_\star = 3.0\ M_\odot$, $M_L = 0.2\ M_\odot$, $D_S = 8.5$ kpc, $D_L = 7.0$ kpc, $u_{\rm min} = 0.5$, $V = 100$ km/s, $\phi = 0^\circ$, $i = 0^\circ$ and $\Omega = 0^\circ$. For comparison, the trajectory and magnification curve of the host star are also shown. The amplitude of the oscillation of the planet's trajectory in y direction is determined by Eq. (3.6). As we see in the right plot, the magnification of the planet waves around that of the host star due to the periodic orbital motion. The maximum magnification of the planet exceeds that of the host star because, as seen in the left panel, the planet approaches the lens more than the host star. In fact, the shape of magnification curve and the maximum magnification depends on the initial orbital phase. Below, we investigate the dependence of the magnification curve on the parameters.

In Fig. 3.3, the variation of the magnification is shown by varying the relative transverse velocity, V, and fixing other parameters. The crossing time shortens for a smaller value of V as in Eq. (3.3) and the magnification curve shrinks in time direction.n Furthermore, the wavy feature in the magnification curve of the tail (magnification $\lesssim 1.5$) is reduced when the transverse velocity becomes comparable or larger than the planet's orbital velocity. In this plot the maximum magnifications are almost the same for the three cases but this depends on the initial phases of the orbital motion again.

Fig. 3.4 compares the trajectory and magnification curve for different values of $u_{\rm min}$. It is seen that a smaller value of $u_{\rm min}$ results in not only overall enhancement of the magnification but also a larger amplitude of the oscillation of the magnification around that of the host star (not shown). This is because the fractional variation of u of the planet becomes larger for a smaller value of $u_{\rm min}$.

The effect of changing the host star mass is shown in Fig. 3.5. A smaller mass leads to a longer orbital period and the number of the oscillation of the magnification is reduced for a fixed crossing time (relative transverse velocity). Similar effect can be seen in Fig. 3.6, where the semi-major axis is varied, because the orbital period depends on the semi-major axis as well. In this case, the y range of the planet trajectory is expanded for a larger value of a, and the maximum magnification is larger.

Finally, Fig. 3.7 compares the cases of face-on ($i = 0^\circ$) and edge-on ($i = 90^\circ$). In the edge-on case, the trajectory is a straight line, but the x-coordinate does not increase monotonically and the planet can move backwards in the lens plane. This is why the magnification oscillates even for the edge-on case, although the wavy feature is smeared substantially. The vertical lines represent the transit of the planet by the host star and the radio emission is diminished there.

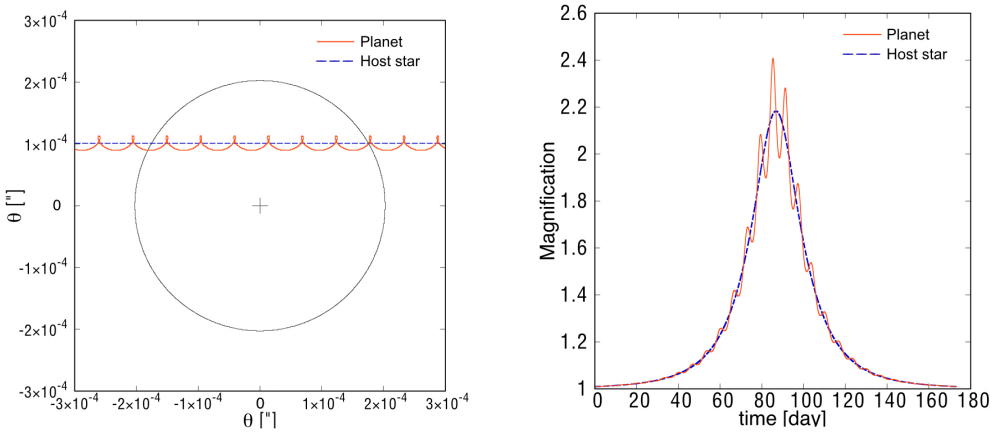

Figure 3.2: Left: trajectories of the planet (solid) and host star (dashed) with parameters, $M_\star = 3.0\ M_\odot$, $M_L = 0.2\ M_\odot$, $D_S = 8.5$ kpc, $D_L = 7.0$ kpc, $a = 0.1$ AU, $u_{\rm min} = 0.5$, $V = 100$ km/s, $\phi = 0°$, $i = 0°$ and $\Omega = 0°$. The lens is located at the origin and the circle represents the Einstein radius. Right: corresponding magnification curves.

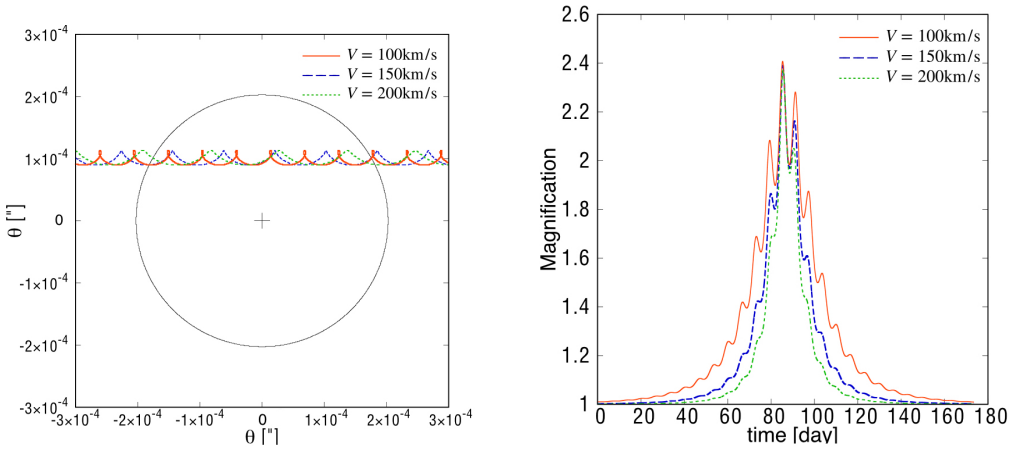

Figure 3.3: Same as Fig. 3.2 but varying the relative transverse velocity, V. The red solid line, blue dashed line and green dotted line cofrespond to $V = 100$ km/s, $V = 150$ km/s and $V = 200$ km/s, respectively.

As we have seen, a source planet with a relatively small semi-major axis, and then a short orbital period, can have a unique wavy feature in the magnification curve, depending on the parameters. The feature is useful for not only the identification of microlensing event of exoplanets but estimation of the fundamental parameters of the planetary system. However, these wavy features cannot be seen when the orbital period is comparable to or longer than the crossing time. In this case, the magnification curve would be very similar to normal microlensing events. Nevertheless, microlensing will be very useful to observe faint radio signals from distant exoplanets.

3.3 Event rate

In this section, we investigate the observability of the radio emission from exoplanets amplified by gravitational microlensing and estimate the event rate. We consider the microlensing events toward the Galactic Center because the event rate is expected to be relatively high in the direction. In fact, the SKA is planning surveys of the Galactic Center and Galactic plane with a survey time of order $O(1000)$ hours. They are commensal

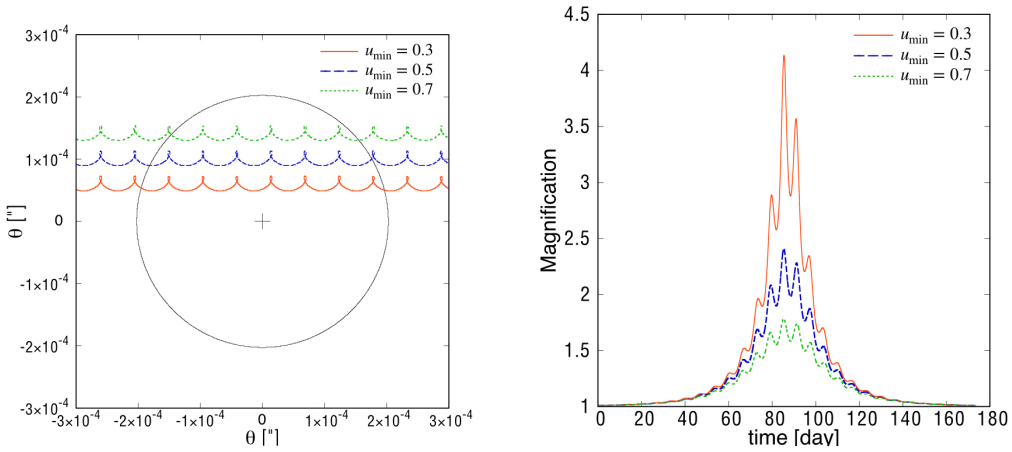

Figure 3.4: Same as Fig. 3.2 but varying $u_{\rm min}$. The red solid line, blue dashed line and green dotted line correspond to $u_{\rm min} = 0.3$, $u_{\rm min} = 0.5$ and $u_{\rm min} = 0.7$, respectively.

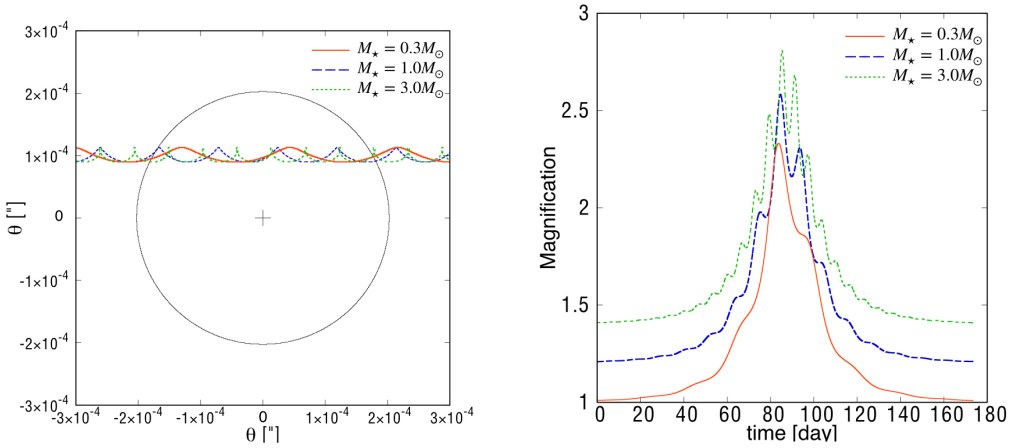

Figure 3.5: Same as Fig. 3.2 but varying the host star mass $M_\star$. The red solid line, blue dashed line and green dotted line correspond to $M_\star = 0.3\ M_\odot$, $M_\star = 1.0\ M_\odot$ and $M_\star = 3.0\ M_\odot$, respectively. In the right panel, the blue dashed line and green dotted line are shifted upward by 0.2 and 0.4, respectively.

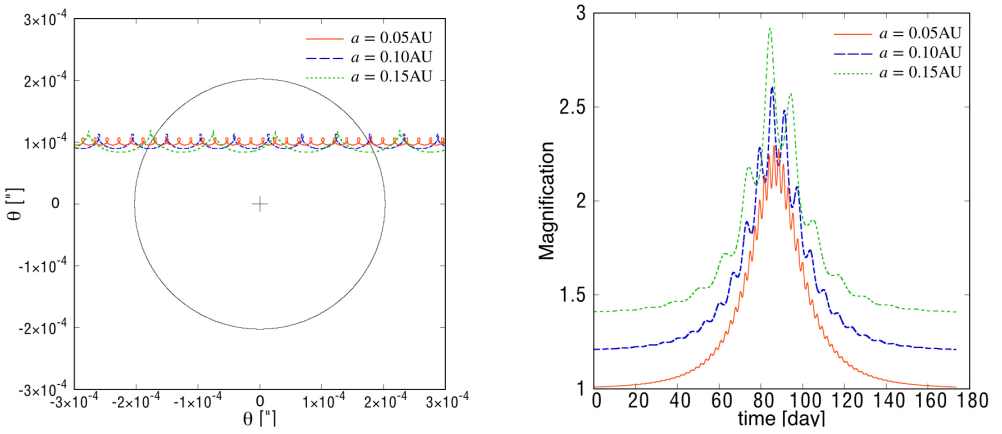

Figure 3.6: Same as Fig. 3.2 but varying the semi-major axis a. The red solid line, blue dashed line and green dotted line correspond to $a = 0.05$ AU, $a = 0.10$ AU and $a = 0.15$ AU, respectively. In the right panel, the blue dashed line and green dotted line are shifted upward by 0.2 and 0.4, respectively.

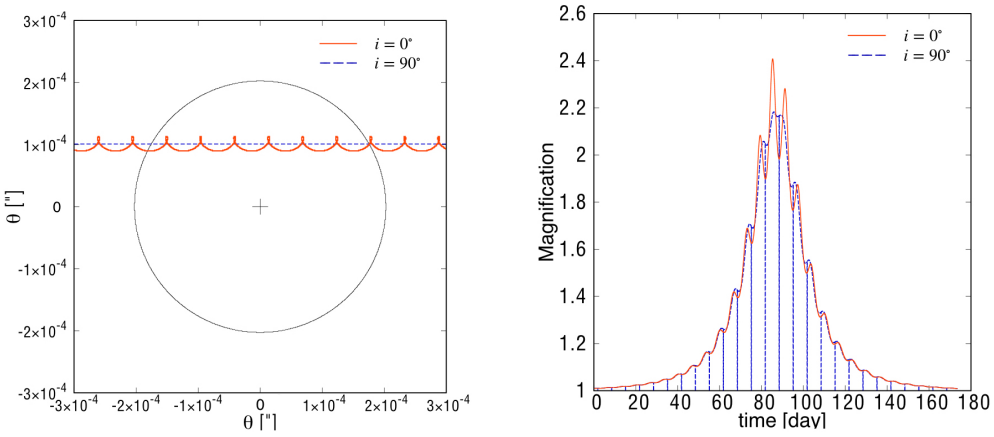

Figure 3.7: Same as Fig. 3.2 but varying the inclination i. The red solid line and blue dashed line correspond to $i = 0°$ (face-on) and $i = 90°$ (edge-on), respectively. In the right panel, the vertical lines represent the transit of the planet by the host star.

surveys so that the data can be used for various scientific purposes. We assume to use the data of such large commensal surveys to search for microlensing events. However, the microlensed sources in the direction of Galactic Center are mostly located at the bulge region with a typical distance of 7 kpc. Thus, the radio emission is very faint and, as we will see, a magnification of an order of O(100) is required to be detected even with the SKA.

We can estimate the event rate of microlensing of hot Jupiters by multiplying the following factors.

1. S [deg^2]: area of survey field
2. $R_{\rm lens}$ [/year/deg^2]: event rate of microlensing of stars
3. $P_{\rm HJ}$: probability that a star has a hot Jupiter
4. $P_{\rm obs}$: conditional probability that the peak luminosity of a hot Jupiter reaches the detection threshold given that the host star enters the Einstein ring of a lens star

In this study, we assume a survey area of $S = 100$ [deg^2]. We estimate $R_{\rm lens} \sim 100/{\rm year/deg}^2$ in the direction of Galactic Center, based on Mróz et al. [2019]. The occurrence of a hot Jupiter around FGK stars has been estimated to be $P_{\rm HJ} \sim 1\%$ [Mayor et al., 2011, Wright et al., 2012, Fressin et al., 2013]. The remaining number to estimate is $P_{\rm obs}$.

Below, we evaluate $P_{\rm obs}$ through a Monte-Carlo method considering the variation of the 9 parameters given in the previous section and the emissivity of exoplanets. To do this, we need to determine the radio power of an exoplanet given a set of parameters. It is suggested that the radio power is proportional to the incident power of stellar wind into the planet's magnetosphere [e.g., Zarka, 1992, Zarka et al., 1997]. Thus, the radio power may naively be assumed to be proportional to a geometric factor of a^{-2}. However, as a decreases, the kinetic and magnetic pressure of the stellar wind increases, and the planet's magnetosphere would shrink and the incident power may not increase so rapidly. Considering this effect, the radio power would be proportional to $a^{-4/3}$ [e.g., Grießmeier et al., 2005]. Although there are other scaling laws suggested in the literature [Farrell et al., 1999, Zarka et al., 2001, Lazio et al., 2004], we consider the above two cases (a^{-2}, $a^{-4/3}$) as typical scaling laws. Concerning the overall normalization of radio power, we take Jupiter's one ($P_{\rm rad} = 10^{11}$ W at $a = 5$ AU). Thus, because most of

observable exoplanets have a very small semi-major axis ($\lesssim 0.1$ AU) as we will see later, our targets are mostly hot Jupiters.

In this study, we consider using the SKA1-LOW that will have a high sensitivity of 70 μJy at 50 MHz with 4 MHz $\times$ 1 hour integration [Zarka et al., 2015]. A deeper and wider-band observation (40 MHz $\times$ 10 hours integration, designated as "SKA1-LOW Deep") is also considered. As a comparison, we evaluate the potential of observations by the LOFAR with sensitivity which is about 1/30 of the SKA1-LOW at 50 MHz. Thus, for example, an exoplanet with $a = 0.05$ AU at 1 (7) kpc needs a magnification of a factor of ~ 60 (2800) to be detectable by SKA1-LOW Deep.

In fact, the highest frequency of Jupiter's auroral radio emission is ~ 30 MHz and outside the frequency range of the SKA1-LOW. However, the highest frequency is proportional to the magnitude of the surface magnetic field (12 Gauss for Jupiter) and even stronger magnetic fields are expected for hot Jupiters [e.g., Cauley et al., 2019]. Thus, we assume exoplanet's radio emission extends beyond 50 MHz, which is possible if the surface field is stronger than 20 Gauss.

Based on the above assumptions, we can study the detectability of radio emission from exoplanets. First, we discuss the dependence on the detectability in the a-$u_{\rm min}$ plane (Fig. 3.8). For this, we make 19997 parameter sets by randomly choosing a, $u_{\rm min}$ (random in the logarithmic scale), ϕ, i and Ω (random in the linear scale) while fixing other parameters such that $M_\star = 1.0\ M_\odot$, $M_L = 1.0\ M_\odot$, $D_S = 7.0$ kpc, $D_L = 3.5$ kpc and $V = 200$ km/s. Then, for each parameter set, we ask if (i) the amplified radio emission is above the sensitivity of SKA1-LOW Deep, and (ii) if the magnification curve has multiple peaks and the characteristic wavy features, which would be needed to identify the planetary nature of the emission. For the scaling of radio emissivity, we adopt the a^{-2} law. The upper panel of Fig. 3.8 represents the scatter plot where the blue crosses correspond to the parameter sets that satisfy both criteria with SKA1-LOW Deep, i.e., they are detectable by SKA1-LOW Deep with wavy features. On the other hand, red points represents the parameter sets that satisfy the first criterion only, i.e., the radio power is detectable but the wavy patterns are not seen. The typical value of $u_{\rm min}$ is 10^{-2}, which corresponds to a magnification factor of $\sim 1/u_{\rm min} \sim 100$.

Generally, in order for an exoplanet to be detectable, values of a and/or $u_{\rm min}$ must are smaller than figures described in section 2 because they give a large intrinsic luminosity and large magnification, respectively. If the orbital motion of a planet is ignored, the peak luminosity scales as $a^{-2}u_{\rm min}$. Therefore, planets under a line $a^{-2}u_{\rm min} = $ const., which goes from up-left to bottom-right in the upper panel of Fig. 3.8, are detectable for most of other random parameter sets (ϕ, i and Ω) (see the lower panel). In this case, as we can see, the magnification curve often has multiple peaks.

On the other hand, we see that many planets just above the line are still detectable with the probability of $O(10)\%$. Interestingly, at $u_{\rm min} \approx 10^{-2}$, there are a few detectable planets with $a > 0.05$ AU, while no planets with 0.05 AU $> a > 0.01$ AU are found. This is apparently strange because the intrinsic luminosity is larger for planets with 0.05 AU $> a > 0.01$ AU. In fact, for $a > 0.05$ AU, the angular scale of the semi-major axis is as large as $u_{\rm min}$ (see Eq. (3.6)) so that the planet can be very close to the lens star depending on the initial orbital phase. Thus, planets with $a > 0.05$ AU can have very large magnification of $O(1000)$ and become detectable even if the intrinsic luminosity is relatively low.

Finally, Fig. 3.9 shows the conditional probability, $P_{\rm obs}$, that an exoplanet can be detected as a function of the source distance, given that the host star enters the Einstein radius of a lens star. Red, blue and green curves represent SKA1-LOW Deep, SKA1-LOW and LOFAR, respectively. In upper and lower panels, the scaling law of $P_{\rm rad} \propto a^{-2}$ and $a^{-4/3}$ are assumed, respectively. In upper and lower panels, the lens mass is set to 0.1 $M_\odot$ and 1.0 $M_\odot$, respectively. For simplicity, the lens distance is set to the

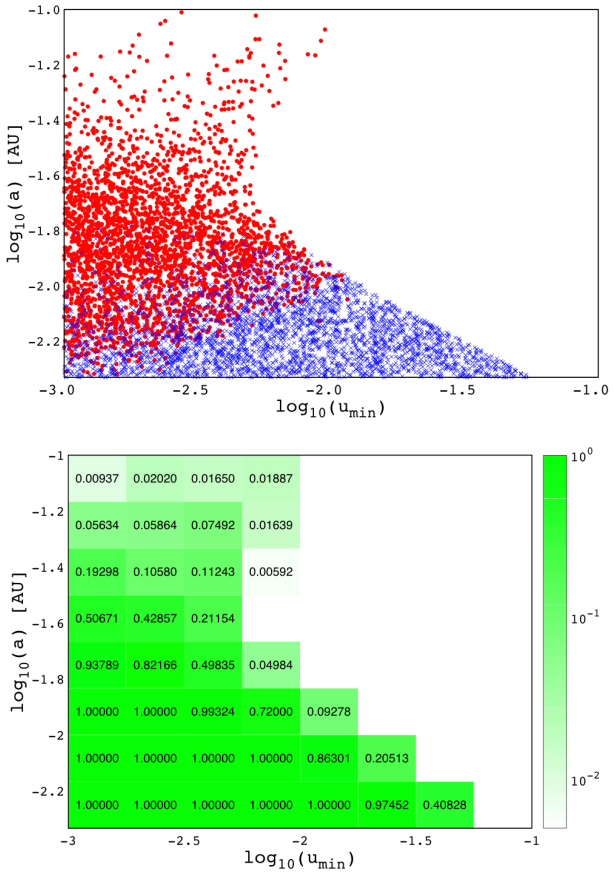

Figure 3.8: Upper panel: scatter plot of exoplanets detectable with SKA1-LOW Deep (40MHz $\times$ 10 hours integration) assuming a scaling law of a^{-2}. Four of the parameters, a, $u_{\rm min}$, ϕ, i and Ω are randomly chosen, while other parameters are set as $M_\star = 1.0\ M_\odot$, $M_L = 1.0\ M_\odot$, $D_S = 7.0$ kpc, $D_L = 3.5$ kpc and $V = 200$ km/s. Blue and red points represent planets whose magnification curves have multiple peaks and a single peak, respectively. Lower panel: probability of the detection for each region in a-$u_{\rm min}$ plane.

half of the source distance. The semi-major axis is chosen randomly according to a probability distribution function derived from the observed hot-Jupiter population (0.00263 AU – 0.1 AU) [2], which is close to Gaussian distribution with mean of 0.05 AU and standard deviation of 0.02 AU. The values of $u_{\rm min}$, ϕ, i and Ω are randomly chosen from uniform probability distributions. Other parameters are set as $M_\star = 1.0\ M_\odot$ and $V = 200$ km/s.

It is seen that the probability does not depend largely on the lens mass. This is because the magnification is determined by u, which is the relative angle between the source and lens normalized by the Einstein radius. Therefore, although the probability that a source is microlensed increases as the lens mass increases, the conditional probability of the current interest is not affected. On the other hand, the observability strongly depends on the scaling law. In fact, the difference in the radio emissivity at 0.05 AU is a factor of 20 between the two scaling laws, noting that it is normalized by Jupiter at 5 AU.

To estimate the event rate of microlensing of hot Jupiters, we focus on exoplanets located at the bulge region, which will dominate microlensing events toward the Galactic Center. Then, we take $P_{\rm obs} = 3\times10^{-3}$ and 3×10^{-5} as typical probabilities for exoplanets with scaling law of a^{-2} and $a^{-4/3}$, respectively, considering the SKA1-LOW Deep

[2] *http://exoplanet.eu*

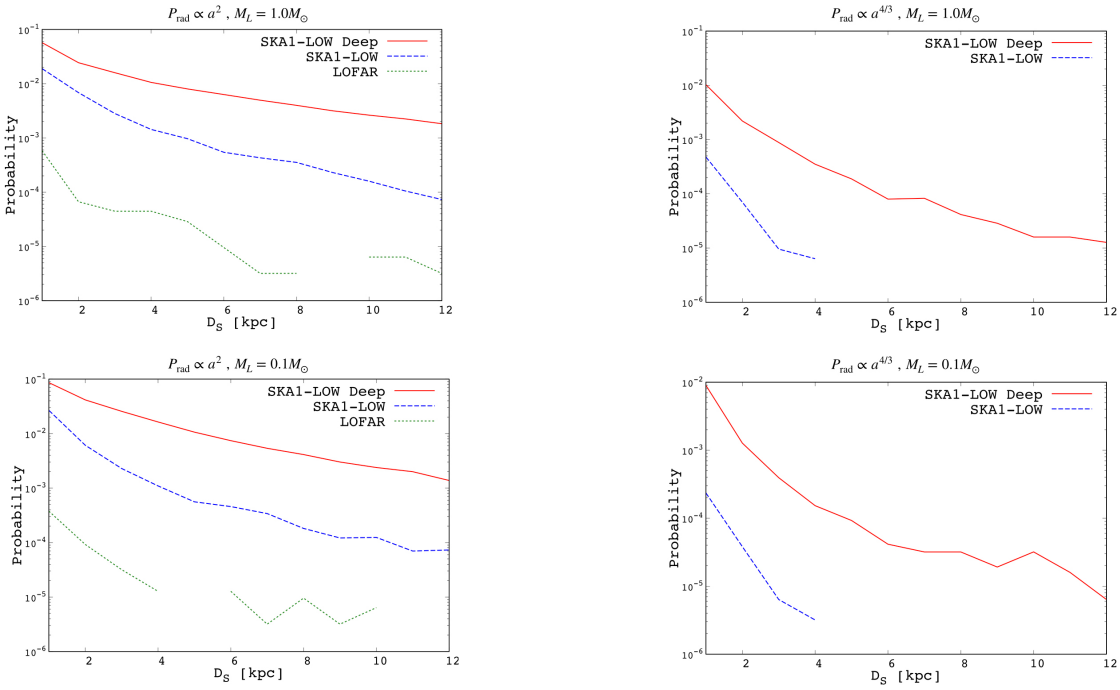

Figure 3.9: Conditional probability that an exoplanet can be detected as a function of the distance, D_S, given that the host star enters the Einstein radius of a lens star. In upper and lower panels, the scaling law of $P_{\rm rad} \propto a^{-2}$ and $a^{-4/3}$ are assumed, respectively. In left and right panels, the lens mass is set to 0.1 $M_\odot$ and 1.0 $M_\odot$, respectively. Here, the lens distance is set to the half of the source distance. The semi-major axis is chosen randomly according to a probability distribution function derived from the observed population. The values of $u_{\rm min}$, ϕ, i and Ω are randomly chosen from uniform probability distributions. Other parameters are set as $M_\star = 1.0\ M_\odot$ and $V = 200$ km/s. Red, blue and green curves represent SKA1-LOW Deep, SKA1-LOW and LOFAR, respectively.

observation. In this case, we have an event rate of $R_{\rm lens} \times P_{\rm HJ} \times P_{\rm obs} \times S \approx 0.3$ year^{-1} and 0.003 year^{-1} for a^{-2} and $a^{-4/3}$ scalings, respectively. In case of SKA1-LOW and LOFAR, the expected event rates are lower than the above by about a factor of 10 and 300, respectively.

3.4 Discussion

In this paper, we studied microlensing of a exoplanetary system as a source, not as a lensing object. This enhances the detectability of the radio emission which allows us to probe the activity of the planet's magnetosphere [Hess and Zarka, 2011, Zarka et al., 2015]. Due to the orbital motion of the exoplanet around the host star, if the semi-major axis is relatively small ($\lesssim 0.1$ AU), the magnification curve has a wavy feature which reflects the orbital parameters and masses of the host and lens stars. This is a unique feature which can be used to identify microlensing event of an exoplanet.

Auroral radio emission from exoplanets, especially hot Jupiters, can be much brighter than the host star in low-frequency radio band and can extend to $\gtrsim 50$ MHz for an exoplanet with relatively strong surface magnetic fields ($\gtrsim 20$ Gauss). Thus, auroral radio emission of exoplanets is an intriguing target of the next-generation radio telescopes such as the SKA-LOW, and microlensing can enhance the observability.

We estimated the event rate of microlensing of exoplanets toward Galactic Center region expected with monitoring observations by the SKA1-LOW and LOFAR. It was

found that the expected event rate is as large as 0.03 year^{-1} and 0.3 year^{-1} by SKA1-LOW observation with 4 MHz $\times$ 1 hours and 40 MHz $\times$ 10 hours integrations, respectively. Although the event rate is not high even for the SKA1-LOW, magnification by microlensing gives us a chance to observe distant exoplanets.

Our discussion on observability relied largely on the scaling law of radio emissivity, which is highly uncertain at this time. In addition, while we estimated the auroral radio power by simply scaling the Jupiter's value, it would also be affected by the properties of the stellar wind, and different types of the host stars may have a different normalization. A different scaling law and/or normalization can lead to substantially different results and, conversely, statistics of radio emissivity of exoplanets can be probed from future observations.

It is well known that auroral radio emission of Jupiter and Saturn are highly anisotropic [Lamy et al., 2008]. Therefore, if the radio emission of hot Jupiters are also anisotropic, the event rate will be reduced by a factor of the solid angle of the emission divided by 4π.

In this paper, we considered radio emission from the magnetosphere of exoplanets. Another possible radio emission involving exoplanets is that from the star-planet interaction. Most M dwarfs have short-period planets and M dwarf-planet systems can be promising radio sources [Vedantham et al., 2020]. While microlensing can amplify these systems and enhance the observability, the characteristic wavy feature is not likely to be seen when the dominant radio emission comes from the surface of the host star.

It should be noted that the shape of the light curve of a microlensed hot Jupiter does not necessarily coincide with that of the magnification curve, because the radio emission is expected to have an intrinsic variability. In fact, Jupiter's auroral radio emission varies with its spin period. Nevertheless, if the timescale of intrinsic variability is shorter than the orbital period and crossing time, the wavy feature could still be observed in the light curve. Observation of the magnification curve is very important because the wavy feature contains much information on the system such as the masses of the host and lens stars and the orbital parameters.

In this chapter, we considered only exoplanets as radio sources toward the Galactic Center. Actually, the observation of radio emission from exoplanets could be confusion-limited due to a finite angular resolution of the radio telescopes. To identify exoplanets, the circular polarization is a good measure because most of other sources are expected to be unpolarized. Also, as was shown in our manuscript, micro-lensed exoplanets can be distinguished by the unique feature of the magnification curve if a significant fraction of the light curve, not just the peak, could be observed. Furthermore, if optical data is available, the cross-matching between radio (circular polarization) and optical sources is an effective way to reduce the confusion [Callingham et al., 2019].

The synergy between the radio and optical/infrared observations is a promising way to not only identify micro-lensed exoplanets but constrain their orbital parameters. In fact, as we saw in Fig. 3.2, the magnification curve is different between the host star and the planet, and they will provide us complimentary information. A quantitative discussion on parameter estimation, considering OGLE, MOA and WFIRST as the optical counterparts of the SKA, will be given elsewhere.

Data Availability

The observational data used in this paper can be accessed in the GMRT online archive (https://naps.ncra.tifr.res.in/goa/data/search) under proposal number 38_008.

Acknowledgements

I am extremely grateful to my supervisor, Professor Keitaro Takahashi, for accepting me to start research on exoplanets and for his invaluable advice and continuous support during my PhD life. I am also grateful to my collaborators Dr. Yuka Fujii at the National Astronomical Observatory of Japan, Dr. Hajime Kita at the Tohoku Institute of Technology, Yuka Terada at the National Taiwan University, and Dr. Tomoki Kimura at the Tokyo University of Science. This work would not have been accomplished without the help and advice with them. I would like to thank to all the members, especially to exoplanet group members Shin Akagi (OB), Mika Nakamura (OG), Masatoki Kamiuchi, Konatsu Higashi (OG) and Shintaro Nakao in Keitaro Takahashi ' s laboratory for useful discussion and supports.

This work is supported by Japan Society for the Promotion of Science (JSPS) KAKENHI Grant Number 22KJ251000.

References

A. Antonova, G. Hallinan, J. G. Doyle, S. Yu, A. Kuznetsov, Y. Metodieva, A. Golden, and K. L. Cruz. Volume-limited radio survey of ultracool dwarfs. *Astronomy and Astrophysics*, 549:A131, January 2013. doi: 10.1051/0004-6361/201118583.

Reza Ashtari, Anthony Sciola, Jake D. Turner, and Kevin Stevenson. Detecting Magnetospheric Radio Emission from Giant Exoplanets. *Astrophysical Journal*, 939(1):24, November 2022. doi: 10.3847/1538-4357/ac92f5.

Fatemeh Bagheri, Sedighe Sajadian, and Sohrab Rahvar. Detection of exoplanet as a binary source of microlensing events in WFIRST survey. *Monthly Notices of the Royal Astronomical Society*, 490(2):1581–1587, Dec 2019. doi: 10.1093/mnras/stz2682.

T. S. Bastian, G. A. Dulk, and Y. Leblanc. A Search for Radio Emission from Extrasolar Planets. *Astrophysical Journal*, 545(2):1058–1063, Dec 2000. doi: 10.1086/317864.

T. S. Bastian, J. Villadsen, A. Maps, G. Hallinan, and A. J. Beasley. Radio Emission from the Exoplanetary System ε Eridani. *Astrophysical Journal*, 857(2):133, April 2018. doi: 10.3847/1538-4357/aab3cb.

E. Berger. Flaring up All Over-Radio Activity in Rapidly Rotating Late M and L Dwarfs. *Astrophysical Journal*, 572(1):503–513, June 2002. doi: 10.1086/340301.

E. Berger. Radio Observations of a Large Sample of Late M, L, and T Dwarfs: The Distribution of Magnetic Field Strengths. *Astrophysical Journal*, 648(1):629–636, September 2006. doi: 10.1086/505787.

E. Berger, S. Ball, K. M. Becker, M. Clarke, D. A. Frail, T. A. Fukuda, I. M. Hoffman, R. Mellon, E. Momjian, N. W. Murphy, S. H. Teng, T. Woodruff, B. A. Zauderer, and R. T. Zavala. Discovery of radio emission from the brown dwarf LP944-20. *Nature*, 410(6826):338–340, March 2001. doi: 10.48550/arXiv.astro-ph/0102301.

E. Berger, R. E. Rutledge, I. N. Reid, L. Bildsten, J. E. Gizis, J. Liebert, E. Martín, G. Basri, R. Jayawardhana, A. Brandeker, T. A. Fleming, C. M. Johns-Krull, M. S. Giampapa, S. L. Hawley, and J. H. M. M. Schmitt. The Magnetic Properties of an L Dwarf Derived from Simultaneous Radio, X-Ray, and Hα Observations. *Astrophysical Journal*, 627(2):960–973, July 2005. doi: 10.1086/430343.

E. Berger, R. E. Rutledge, N. Phan-Bao, G. Basri, M. S. Giampapa, J. E. Gizis, J. Liebert, E. Martín, and T. A. Fleming. Periodic Radio and Hα Emission from the L Dwarf Binary 2MASSW J0746425+200032: Exploring the Magnetic Field Topology and Radius Of An L Dwarf. *Astrophysical Journal*, 695(1):310–316, April 2009. doi: 10.1088/0004-637X/695/1/310.

P. M. S. Blackett. The Magnetic Field of Massive Rotating Bodies. *Nature*, 159(4046): 658–666, May 1947. doi: 10.1038/159658a0.

Geoffrey C. Bower, Laurent Loinard, Sergio Dzib, Phillip A. B. Galli, Gisela N. Ortiz-León, Claire Moutou, and Jean-Francois Donati. Variable Radio Emission from the Young Stellar Host of a Hot Jupiter. *Astrophysical Journal*, 830(2):107, October 2016. doi: 10.3847/0004-637X/830/2/107.

Adam J. Burgasser and Mary E. Putman. Quiescent Radio Emission from Southern Late-Type M Dwarfs and a Spectacular Radio Flare from the M8 Dwarf DENIS 1048-3956. *Astrophysical Journal*, 626(1):486–497, June 2005. doi: 10.1086/429788.

Adam J. Burgasser, Carl Melis, B. Ashley Zauderer, and Edo Berger. Detection of Radio Emission from the Hyperactive L Dwarf 2MASS J13153094-2649513AB. *Astrophysical Journal, Letters*, 762(1):L3, January 2013. doi: 10.1088/2041-8205/762/1/L3.

Adam J. Burgasser, Carl Melis, Jacob Todd, Christopher R. Gelino, Gregg Hallinan, and Daniella Bardalez Gagliuffi. Radio Emission and Orbital Motion from the Close-encounter Star-Brown Dwarf Binary WISE J072003.20-084651.2. *Astronomical Journal*, 150(6):180, December 2015. doi: 10.1088/0004-6256/150/6/180.

J. R. Callingham, H. K. Vedantham, B. J. S. Pope, T. W. Shimwell, and LoTSS Team. LoTSS-HETDEX and Gaia: Blind Search for Radio Emission from Stellar Systems Dominated by False Positives. *Research Notes of the American Astronomical Society*, 3(2):37, February 2019. doi: 10.3847/2515-5172/ab07c3.

J. R. Callingham, H. K. Vedantham, T. W. Shimwell, B. J. S. Pope, I. E. Davis, P. N. Best, M. J. Hardcastle, H. J. A. Röttgering, J. Sabater, C. Tasse, R. J. van Weeren, W. L. Williams, P. Zarka, F. de Gasperin, and A. Drabent. The population of M dwarfs observed at low radio frequencies. *Nature Astronomy*, 5:1233–1239, December 2021. doi: 10.1038/s41550-021-01483-0.

P. Wilson Cauley, Evgenya L. Shkolnik, Joe Llama, and Antonino F. Lanza. Magnetic field strengths of hot Jupiters from signals of star-planet interactions. *Nature Astronomy*, 3:1128–1134, Jul 2019. doi: 10.1038/s41550-019-0840-x.

Y. Cendes, P. K. G. Williams, and E. Berger. A Pilot Radio Search for Magnetic Activity in Directly Imaged Exoplanets. *Astronomical Journal*, 163(1):15, January 2022. doi: 10.3847/1538-3881/ac32c8.

Gilles Chabrier and Isabelle Baraffe. Theory of Low-Mass Stars and Substellar Objects. *Annual Review of Astronomy and Astrophysics*, 38:337–377, January 2000. doi: 10.1146/annurev.astro.38.1.337.

Jeffrey Chilcote, Laurent Pueyo, Robert J. De Rosa, Jeffrey Vargas, Bruce Macintosh, Vanessa P. Bailey, Travis Barman, Brian Bauman, Sebastian Bruzzone, Joanna Bulger, Adam S. Burrows, Andrew Cardwell, Christine H. Chen, Tara Cotten, Daren Dillon, Rene Doyon, Zachary H. Draper, Gaspard Duchêne, Jennifer Dunn, Darren Erikson, Michael P. Fitzgerald, Katherine B. Follette, Donald Gavel, Stephen J. Goodsell, James R. Graham, Alexandra Z. Greenbaum, Markus Hartung, Pascale Hibon, Li-Wei Hung, Patrick Ingraham, Paul Kalas, Quinn Konopacky, James E. Larkin, Jérôme Maire, Franck Marchis, Mark S. Marley, Christian Marois, Stanimir Metchev, Maxwell A. Millar-Blanchaer, Katie M. Morzinski, Eric L. Nielsen, Andrew Norton, Rebecca Oppenheimer, David Palmer, Jennifer Patience, Marshall Perrin, Lisa Poyneer, Abhijith Rajan, Julien Rameau, Fredrik T. Rantakyrö, Naru Sadakuni, Leslie Saddlemyer, Dmitry Savransky, Adam C. Schneider, Andrew Serio, Anand Sivaramakrishnan, Inseok Song, Remi Soummer, Sandrine Thomas, J. Kent Wallace, Jason J. Wang, Kimberly Ward-Duong, Sloane Wiktorowicz, and Schuyler Wolff. 1-2.4 μm Near-IR Spectrum of the Giant Planet β Pictoris b Obtained with the Gemini Planet Imager. *Astronomical Journal*, 153(4):182, April 2017. doi: 10.3847/1538-3881/aa63e9.

Ulrich R. Christensen, Volkmar Holzwarth, and Ansgar Reiners. Energy flux determines magnetic field strength of planets and stars. *Nature*, 457(7226):167–169, Jan 2009. doi: 10.1038/nature07626.

Juan B. Climent, J. C. Guirado, M. R. Zapatero-Osorio, O. V. Zakhozhay, M. A. Pérez-Torres, R. Azulay, B. Gauza, R. Rebolo, V. J. S. Béjar, J. Martín-Pintado, and C. Lefèvre. Radio emission in a nearby ultracool dwarf binary: a multi-frequency study. *arXiv e-prints*, art. arXiv:2201.12606, January 2022. doi: 10.48550/arXiv.2201.12606.

S. Daley-Yates and I. R. Stevens. Interacting fields and flows: Magnetic hot Jupiters. *Astronomische Nachrichten*, 338(8):881–884, October 2017. doi: 10.1002/asna.201713395.

S. Daley-Yates and I. R. Stevens. Inhibition of the electron cyclotron maser instability in the dense magnetosphere of a hot Jupiter. *Monthly Notices of the Royal Astronomical Society*, 479(1):1194–1209, September 2018. doi: 10.1093/mnras/sty1652.

F. de Gasperin, T. J. W. Lazio, and M. Knapp. Radio observations of HD 80606 near planetary periastron. II. LOFAR low band antenna observations at 30-78 MHz. *Astronomy and Astrophysics*, 644:A157, December 2020. doi: 10.1051/0004-6361/202038746.

W. M. Farrell, M. D. Desch, and P. Zarka. On the possibility of coherent cyclotron emission from extrasolar planets. *Journal of Geophysics Research*, 104(E6):14025–14032, Jun 1999. doi: 10.1029/1998JE900050.

W. M. Farrell, M. D. Desch, T. J. Lazio, T. Bastian, and P. Zarka. Limits on the Magnetosphere/Stellar Wind Interactions for the Extrasolar Planet about Tau Bootis. In Drake Deming and Sara Seager, editors, *Scientific Frontiers in Research on Extrasolar Planets*, volume 294 of *Astronomical Society of the Pacific Conference Series*, pages 151–156, January 2003.

François Fressin, Guillermo Torres, David Charbonneau, Stephen T. Bryson, Jessie Christiansen, Courtney D. Dressing, Jon M. Jenkins, Lucianne M. Walkowicz, and Natalie M. Batalha. The False Positive Rate of Kepler and the Occurrence of Planets. *Astrophysical Journal*, 766(2):81, Apr 2013. doi: 10.1088/0004-637X/766/2/81.

Yuka Fujii, David S. Spiegel, Tony Mroczkowski, Jason Nordhaus, Neil T. Zimmerman, Aaron R. Parsons, Mehrdad Mirbabayi, and Nikku Madhusudhan. Radio Emission from Red-giant Hot Jupiters. *Astrophysical Journal*, 820(2):122, Apr 2016. doi: 10.3847/0004-637X/820/2/122.

Gaia Collaboration, T. Prusti, J. H. J. de Bruijne, A. G. A. Brown, A. Vallenari, C. Babusiaux, C. A. L. Bailer-Jones, U. Bastian, M. Biermann, D. W. Evans, L. Eyer, F. Jansen, C. Jordi, S. A. Klioner, U. Lammers, L. Lindegren, X. Luri, F. Mignard, D. J. Milligan, C. Panem, V. Poinsignon, D. Pourbaix, S. Randich, G. Sarri, P. Sartoretti, H. I. Siddiqui, C. Soubiran, V. Valette, F. van Leeuwen, N. A. Walton, C. Aerts, F. Arenou, M. Cropper, R. Drimmel, E. Høg, D. Katz, M. G. Lattanzi, W. O'Mullane, E. K. Grebel, A. D. Holland, C. Huc, X. Passot, L. Bramante, C. Cacciari, J. Castañeda, L. Chaoul, N. Cheek, F. De Angeli, C. Fabricius, R. Guerra, J. Hernández, A. Jean-Antoine-Piccolo, E. Masana, R. Messineo, N. Mowlavi, K. Nienartowicz, D. Ordóñez-Blanco, P. Panuzzo, J. Portell, P. J. Richards, M. Riello, G. M. Seabroke, P. Tanga, F. Thévenin, J. Torra, S. G. Els, G. Gracia-Abril, G. Comoretto, M. Garcia-Reinaldos, T. Lock, E. Mercier, M. Altmann, R. Andrae, T. L. Astraatmadja, I. Bellas-Velidis, K. Benson, J. Berthier, R. Blomme, G. Busso, B. Carry, A. Cellino, G. Clementini, S. Cowell, O. Creevey, J. Cuypers, M. Davidson, J. De Ridder, A. de Torres, L. Delchambre, A. Dell'Oro, C. Ducourant, Y. Frémat, M. García-Torres, E. Gosset, J. L. Halbwachs, N. C. Hambly, D. L. Harrison, M. Hauser, D. Hestroffer, S. T. Hodgkin, H. E. Huckle, A. Hutton, G. Jasniewicz, S. Jordan, M. Kontizas, A. J. Korn, A. C. Lanzafame, M. Manteiga, A. Moitinho, K. Muinonen, J. Osinde, E. Pancino, T. Pauwels, J. M. Petit, A. Recio-Blanco, A. C. Robin, L. M. Sarro, C. Siopis, M. Smith, K. W. Smith, A. Sozzetti, W. Thuillot, W. van Reeven, Y. Viala, U. Abbas, A. Abreu Aramburu, S. Accart, J. J. Aguado, P. M. Allan, W. Allasia, G. Altavilla, M. A. Álvarez, J. Alves, R. I. Anderson, A. H. Andrei, E. Anglada Varela, E. Antiche, T. Antoja, S. Antón, B. Arcay, A. Atzei, L. Ayache, N. Bach, S. G. Baker, L. Balaguer-Núñez, C. Barache, C. Barata, A. Barbier, F. Barblan, M. Baroni, D. Barrado y Navascués, M. Barros, M. A. Barstow, U. Becciani, M. Bellazzini, G. Bellei, A. Bello García, V. Belokurov, P. Bendjoya, A. Berihuete, L. Bianchi, O. Bienaymé, F. Billebaud, N. Blagorodnova, S. Blanco-Cuaresma, T. Boch, A. Bombrun, R. Borrachero, S. Bouquillon, G. Bourda, H. Bouy, A. Bragaglia, M. A. Breddels, N. Brouillet, T. Brüsemeister, B. Bucciarelli, F. Budnik, P. Burgess, R. Burgon, A. Burlacu, D. Busonero, R. Buzzi, E. Caffau,

J. Cambras, H. Campbell, R. Cancelliere, T. Cantat-Gaudin, T. Carlucci, J. M. Carrasco, M. Castellani, P. Charlot, J. Charnas, P. Charvet, F. Chassat, A. Chiavassa, M. Clotet, G. Cocozza, R. S. Collins, P. Collins, G. Costigan, F. Crifo, N. J. G. Cross, M. Crosta, C. Crowley, C. Dafonte, Y. Damerdji, A. Dapergolas, P. David, M. David, P. De Cat, F. de Felice, P. de Laverny, F. De Luise, R. De March, D. de Martino, R. de Souza, J. Debosscher, E. del Pozo, M. Delbo, A. Delgado, H. E. Delgado, F. di Marco, P. Di Matteo, S. Diakite, E. Distefano, C. Dolding, S. Dos Anjos, P. Drazinos, J. Durán, Y. Dzigan, E. Ecale, B. Edvardsson, H. Enke, M. Erdmann, D. Escolar, M. Espina, N. W. Evans, G. Eynard Bontemps, C. Fabre, M. Fabrizio, S. Faigler, A. J. Falcão, M. Farràs Casas, F. Faye, L. Federici, G. Fedorets, J. Fernández-Hernández, P. Fernique, A. Fienga, F. Figueras, F. Filippi, K. Findeisen, A. Fonti, M. Fouesneau, E. Fraile, M. Fraser, J. Fuchs, R. Furnell, M. Gai, S. Galleti, L. Galluccio, D. Garabato, F. García-Sedano, P. Garé, A. Garofalo, N. Garralda, P. Gavras, J. Gerssen, R. Geyer, G. Gilmore, S. Girona, G. Giuffrida, M. Gomes, A. González-Marcos, J. González-Núñez, J. J. González-Vidal, M. Granvik, A. Guerrier, P. Guillout, J. Guiraud, A. Gúrpide, R. Gutiérrez-Sánchez, L. P. Guy, R. Haigron, D. Hatzidimitriou, M. Haywood, U. Heiter, A. Helmi, D. Hobbs, W. Hofmann, B. Holl, G. Holland, J. A. S. Hunt, A. Hypki, V. Icardi, M. Irwin, G. Jevardat de Fombelle, P. Jofré, P. G. Jonker, A. Jorissen, F. Julbe, A. Karampelas, A. Kochoska, R. Kohley, K. Kolenberg, E. Kontizas, S. E. Koposov, G. Kordopatis, P. Koubsky, A. Kowalczyk, A. Krone-Martins, M. Kudryashova, I. Kull, R. K. Bachchan, F. Lacoste-Seris, A. F. Lanza, J. B. Lavigne, C. Le Poncin-Lafitte, Y. Lebreton, T. Lebzelter, S. Leccia, N. Leclerc, I. Lecoeur-Taibi, V. Lemaitre, H. Lenhardt, F. Leroux, S. Liao, E. Licata, H. E. P. Lindstrøm, T. A. Lister, E. Livanou, A. Lobel, W. Löffler, M. López, A. Lopez-Lozano, D. Lorenz, T. Loureiro, I. MacDonald, T. Magalhães Fernandes, S. Managau, R. G. Mann, G. Mantelet, O. Marchal, J. M. Marchant, M. Marconi, J. Marie, S. Marinoni, P. M. Marrese, G. Marschalkó, D. J. Marshall, J. M. Martín-Fleitas, M. Martino, N. Mary, G. Matijevič, T. Mazeh, P. J. McMillan, S. Messina, A. Mestre, D. Michalik, N. R. Millar, B. M. H. Miranda, D. Molina, R. Molinaro, M. Molinaro, L. Molnár, M. Moniez, P. Montegriffo, D. Monteiro, R. Mor, A. Mora, R. Morbidelli, T. Morel, S. Morgenthaler, T. Morley, D. Morris, A. F. Mulone, T. Muraveva, I. Musella, J. Narbonne, G. Nelemans, L. Nicastro, L. Noval, C. Ordénovic, J. Ordieres-Meré, P. Osborne, C. Pagani, I. Pagano, F. Pailler, H. Palacin, L. Palaversa, P. Parsons, T. Paulsen, M. Pecoraro, R. Pedrosa, H. Pentikäinen, J. Pereira, B. Pichon, A. M. Piersimoni, F. X. Pineau, E. Plachy, G. Plum, E. Poujoulet, A. Prša, L. Pulone, S. Ragaini, S. Rago, N. Rambaux, M. Ramos-Lerate, P. Ranalli, G. Rauw, A. Read, S. Regibo, F. Renk, C. Reylé, R. A. Ribeiro, L. Rimoldini, V. Ripepi, A. Riva, G. Rixon, M. Roelens, M. Romero-Gómez, N. Rowell, F. Royer, A. Rudolph, L. Ruiz-Dern, G. Sadowski, T. Sagristà Sellés, J. Sahlmann, J. Salgado, E. Salguero, M. Sarasso, H. Savietto, A. Schnorhk, M. Schultheis, E. Sciacca, M. Segol, J. C. Segovia, D. Segransan, E. Serpell, I. C. Shih, R. Smareglia, R. L. Smart, C. Smith, E. Solano, F. Solitro, R. Sordo, S. Soria Nieto, J. Souchay, A. Spagna, F. Spoto, U. Stampa, I. A. Steele, H. Steidelmüller, C. A. Stephenson, H. Stoev, F. F. Suess, M. Süveges, J. Surdej, L. Szabados, E. Szegedi-Elek, D. Tapiador, F. Taris, G. Tauran, M. B. Taylor, R. Teixeira, D. Terrett, B. Tingley, S. C. Trager, C. Turon, A. Ulla, E. Utrilla, G. Valentini, A. van Elteren, E. Van Hemelryck, M. van Leeuwen, M. Varadi, A. Vecchiato, J. Veljanoski, T. Via, D. Vicente, S. Vogt, H. Voss, V. Votruba, S. Voutsinas, G. Walmsley, M. Weiler, K. Weingrill, D. Werner, T. Wevers, G. Whitehead, L. Wyrzykowski, A. Yoldas, M. Žerjal, S. Zucker, C. Zurbach, T. Zwitter, A. Alecu, M. Allen, C. Allende Prieto, A. Amorim, G. Anglada-Escudé, V. Arsenijevic, S. Azaz, P. Balm, M. Beck, H. H. Bernstein, L. Bigot, A. Bijaoui, C. Blasco, M. Bonfigli, G. Bono, S. Boudreault, A. Bressan, S. Brown, P. M. Brunet, P. Bunclark, R. Buonanno, A. G.

Butkevich, C. Carret, C. Carrion, L. Chemin, F. Chéreau, L. Corcione, E. Darmigny, K. S. de Boer, P. de Teodoro, P. T. de Zeeuw, C. Delle Luche, C. D. Domingues, P. Dubath, F. Fodor, B. Frézouls, A. Fries, D. Fustes, D. Fyfe, E. Gallardo, J. Gallegos, D. Gardiol, M. Gebran, A. Gomboc, A. Gómez, E. Grux, A. Gueguen, A. Heyrovsky, J. Hoar, G. Iannicola, Y. Isasi Parache, A. M. Janotto, E. Joliet, A. Jonckheere, R. Keil, D. W. Kim, P. Klagyivik, J. Klar, J. Knude, O. Kochukhov, I. Kolka, J. Kos, A. Kutka, V. Lainey, D. LeBouquin, C. Liu, D. Loreggia, V. V. Makarov, M. G. Marseille, C. Martayan, O. Martinez-Rubi, B. Massart, F. Meynadier, S. Mignot, U. Munari, A. T. Nguyen, T. Nordlander, P. Ocvirk, K. S. O'Flaherty, A. Olias Sanz, P. Ortiz, J. Osorio, D. Oszkiewicz, A. Ouzounis, M. Palmer, P. Park, E. Pasquato, C. Peltzer, J. Peralta, F. Péturaud, T. Pieniluoma, E. Pigozzi, J. Poels, G. Prat, T. Prod'homme, F. Raison, J. M. Rebordao, D. Risquez, B. Rocca-Volmerange, S. Rosen, M. I. Ruiz-Fuertes, F. Russo, S. Sembay, I. Serraller Vizcaino, A. Short, A. Siebert, H. Silva, D. Sinachopoulos, E. Slezak, M. Soffel, D. Sosnowska, V. Straižys, M. ter Linden, D. Terrell, S. Theil, C. Tiede, L. Troisi, P. Tsalmantza, D. Tur, M. Vaccari, F. Vachier, P. Valles, W. Van Hamme, L. Veltz, J. Virtanen, J. M. Wallut, R. Wichmann, M. I. Wilkinson, H. Ziaeepour, and S. Zschocke. The Gaia mission. *Astronomy and Astrophysics*, 595:A1, November 2016. doi: 10.1051/0004-6361/201629272.

Gaia Collaboration, A. G. A. Brown, A. Vallenari, T. Prusti, J. H. J. de Bruijne, C. Babusiaux, C. A. L. Bailer-Jones, M. Biermann, D. W. Evans, L. Eyer, F. Jansen, C. Jordi, S. A. Klioner, U. Lammers, L. Lindegren, X. Luri, F. Mignard, C. Panem, D. Pourbaix, S. Randich, P. Sartoretti, H. I. Siddiqui, C. Soubiran, F. van Leeuwen, N. A. Walton, F. Arenou, U. Bastian, M. Cropper, R. Drimmel, D. Katz, M. G. Lattanzi, J. Bakker, C. Cacciari, J. Castañeda, L. Chaoul, N. Cheek, F. De Angeli, C. Fabricius, R. Guerra, B. Holl, E. Masana, R. Messineo, N. Mowlavi, K. Nienartowicz, P. Panuzzo, J. Portell, M. Riello, G. M. Seabroke, P. Tanga, F. Thévenin, G. Gracia-Abril, G. Comoretto, M. Garcia-Reinaldos, D. Teyssier, M. Altmann, R. Andrae, M. Audard, I. Bellas-Velidis, K. Benson, J. Berthier, R. Blomme, P. Burgess, G. Busso, B. Carry, A. Cellino, G. Clementini, M. Clotet, O. Creevey, M. Davidson, J. De Ridder, L. Delchambre, A. Dell'Oro, C. Ducourant, J. Fernández-Hernández, M. Fouesneau, Y. Frémat, L. Galluccio, M. García-Torres, J. González-Núñez, J. J. González-Vidal, E. Gosset, L. P. Guy, J. L. Halbwachs, N. C. Hambly, D. L. Harrison, J. Hernández, D. Hestroffer, S. T. Hodgkin, A. Hutton, G. Jasniewicz, A. Jean-Antoine-Piccolo, S. Jordan, A. J. Korn, A. Krone-Martins, A. C. Lanzafame, T. Lebzelter, W. Löffler, M. Manteiga, P. M. Marrese, J. M. Martín-Fleitas, A. Moitinho, A. Mora, K. Muinonen, J. Osinde, E. Pancino, T. Pauwels, J. M. Petit, A. Recio-Blanco, P. J. Richards, L. Rimoldini, A. C. Robin, L. M. Sarro, C. Siopis, M. Smith, A. Sozzetti, M. Süveges, J. Torra, W. van Reeven, U. Abbas, A. Abreu Aramburu, S. Accart, C. Aerts, G. Altavilla, M. A. Álvarez, R. Alvarez, J. Alves, R. I. Anderson, A. H. Andrei, E. Anglada Varela, E. Antiche, T. Antoja, B. Arcay, T. L. Astraatmadja, N. Bach, S. G. Baker, L. Balaguer-Núñez, P. Balm, C. Barache, C. Barata, D. Barbato, F. Barblan, P. S. Barklem, D. Barrado, M. Barros, M. A. Barstow, S. Bartholomé Muñoz, J. L. Bassilana, U. Becciani, M. Bellazzini, A. Berihuete, S. Bertone, L. Bianchi, O. Bienaymé, S. Blanco-Cuaresma, T. Boch, C. Boeche, A. Bombrun, R. Borrachero, D. Bossini, S. Bouquillon, G. Bourda, A. Bragaglia, L. Bramante, M. A. Breddels, A. Bressan, N. Brouillet, T. Brüsemeister, E. Brugaletta, B. Bucciarelli, A. Burlacu, D. Busonero, A. G. Butkevich, R. Buzzi, E. Caffau, R. Cancelliere, G. Cannizzaro, T. Cantat-Gaudin, R. Carballo, T. Carlucci, J. M. Carrasco, L. Casamiquela, M. Castellani, A. Castro-Ginard, P. Charlot, L. Chemin, A. Chiavassa, G. Cocozza, G. Costigan, S. Cowell, F. Crifo, M. Crosta, C. Crowley, J. Cuypers, C. Dafonte, Y. Damerdji, A. Dapergolas, P. David, M. David, P. de Laverny, F. De Luise, R. De March, D. de Martino, R. de Souza, A. de Torres, J. Debosscher, E. del Pozo, M. Delbo, A. Del-

gado, H. E. Delgado, P. Di Matteo, S. Diakite, C. Diener, E. Distefano, C. Dolding, P. Drazinos, J. Durán, B. Edvardsson, H. Enke, K. Eriksson, P. Esquej, G. Eynard Bontemps, C. Fabre, M. Fabrizio, S. Faigler, A. J. Falcão, M. Farràs Casas, L. Federici, G. Fedorets, P. Fernique, F. Figueras, F. Filippi, K. Findeisen, A. Fonti, E. Fraile, M. Fraser, B. Frézouls, M. Gai, S. Galleti, D. Garabato, F. García-Sedano, A. Garofalo, N. Garralda, A. Gavel, P. Gavras, J. Gerssen, R. Geyer, P. Giacobbe, G. Gilmore, S. Girona, G. Giuffrida, F. Glass, M. Gomes, M. Granvik, A. Gueguen, A. Guerrier, J. Guiraud, R. Gutiérrez-Sánchez, R. Haigron, D. Hatzidimitriou, M. Hauser, M. Haywood, U. Heiter, A. Helmi, J. Heu, T. Hilger, D. Hobbs, W. Hofmann, G. Holland, H. E. Huckle, A. Hypki, V. Icardi, K. Janßen, G. Jevardat de Fombelle, P. G. Jonker, Á. L. Juhász, F. Julbe, A. Karampelas, A. Kewley, J. Klar, A. Kochoska, R. Kohley, K. Kolenberg, M. Kontizas, E. Kontizas, S. E. Koposov, G. Kordopatis, Z. Kostrzewa-Rutkowska, P. Koubsky, S. Lambert, A. F. Lanza, Y. Lasne, J. B. Lavigne, Y. Le Fustec, C. Le Poncin-Lafitte, Y. Lebreton, S. Leccia, N. Leclerc, I. Lecoeur-Taibi, H. Lenhardt, F. Leroux, S. Liao, E. Licata, H. E. P. Lindstrøm, T. A. Lister, E. Livanou, A. Lobel, M. López, S. Managau, R. G. Mann, G. Mantelet, O. Marchal, J. M. Marchant, M. Marconi, S. Marinoni, G. Marschalkó, D. J. Marshall, M. Martino, G. Marton, N. Mary, D. Massari, G. Matijevič, T. Mazeh, P. J. McMillan, S. Messina, D. Michalik, N. R. Millar, D. Molina, R. Molinaro, L. Molnár, P. Montegriffo, R. Mor, R. Morbidelli, T. Morel, D. Morris, A. F. Mulone, T. Muraveva, I. Musella, G. Nelemans, L. Nicastro, L. Noval, W. O'Mullane, C. Ordénovic, D. Ordóñez-Blanco, P. Osborne, C. Pagani, I. Pagano, F. Pailler, H. Palacin, L. Palaversa, A. Panahi, M. Pawlak, A. M. Piersimoni, F. X. Pineau, E. Plachy, G. Plum, E. Poggio, E. Poujoulet, A. Prša, L. Pulone, E. Racero, S. Ragaini, N. Rambaux, M. Ramos-Lerate, S. Regibo, C. Reylé, F. Riclet, V. Ripepi, A. Riva, A. Rivard, G. Rixon, T. Roegiers, M. Roelens, M. Romero-Gómez, N. Rowell, F. Royer, L. Ruiz-Dern, G. Sadowski, T. Sagristà Sellés, J. Sahlmann, J. Salgado, E. Salguero, N. Sanna, T. Santana-Ros, M. Sarasso, H. Savietto, M. Schultheis, E. Sciacca, M. Segol, J. C. Segovia, D. Ségransan, I. C. Shih, L. Siltala, A. F. Silva, R. L. Smart, K. W. Smith, E. Solano, F. Solitro, R. Sordo, S. Soria Nieto, J. Souchay, A. Spagna, F. Spoto, U. Stampa, I. A. Steele, H. Steidelmüller, C. A. Stephenson, H. Stoev, F. F. Suess, J. Surdej, L. Szabados, E. Szegedi-Elek, D. Tapiador, F. Taris, G. Tauran, M. B. Taylor, R. Teixeira, D. Terrett, P. Teyssandier, W. Thuillot, A. Titarenko, F. Torra Clotet, C. Turon, A. Ulla, E. Utrilla, S. Uzzi, M. Vaillant, G. Valentini, V. Valette, A. van Elteren, E. Van Hemelryck, M. van Leeuwen, M. Vaschetto, A. Vecchiato, J. Veljanoski, Y. Viala, D. Vicente, S. Vogt, C. von Essen, H. Voss, V. Votruba, S. Voutsinas, G. Walmsley, M. Weiler, O. Wertz, T. Wevers, L. Wyrzykowski, A. Yoldas, M. Žerjal, H. Ziaeepour, J. Zorec, S. Zschocke, S. Zucker, C. Zurbach, and T. Zwitter. Gaia Data Release 2. Summary of the contents and survey properties. *Astronomy and Astrophysics*, 616:A1, August 2018. doi: 10.1051/0004-6361/201833051.

Samuel J. George and Ian R. Stevens. Giant Metrewave Radio Telescope low-frequency observations of extrasolar planetary systems. *Monthly Notices of the Royal Astronomical Society*, 382(1):455–460, Nov 2007. doi: 10.1111/j.1365-2966.2007.12387.x.

John E. Gizis, Peter K. G. Williams, Adam J. Burgasser, Mattia Libralato, Domenico Nardiello, Giampaolo Piotto, Luigi R. Bedin, Edo Berger, and Rishi Paudel. WISEP J060738.65+242953.4: A Nearby Pole-on L8 Brown Dwarf with Radio Emission. *Astronomical Journal*, 152(5):123, November 2016. doi: 10.3847/0004-6256/152/5/123.

David S. Graff and B. Scott Gaudi. Direct Detection of Large Close-in Planets around the Source Stars of Caustic-crossing Microlensing Events. *Astrophysical Journal, Letters*, 538(2):L133–L136, Aug 2000. doi: 10.1086/312811.

R. O. Gray, C. J. Corbally, R. F. Garrison, M. T. McFadden, E. J. Bubar, C. E. McGahee,

A. A. O'Donoghue, and E. R. Knox. Contributions to the Nearby Stars (NStars) Project: Spectroscopy of Stars Earlier than M0 within 40 pc-The Southern Sample. *Astronomical Journal*, 132(1):161–170, July 2006. doi: 10.1086/504637.

D. A. Green and N. Madhusudhan. Search for radio emission from the exoplanets Qatar-1b and WASP-80b near 150 MHz using the giant metrewave radio telescope. *Monthly Notices of the Royal Astronomical Society*, 500(1):211–214, January 2021. doi: 10.1093/mnras/staa3208.

J. M. Griessmeier. The search for radio emission from giant exoplanets. In G. Fischer, G. Mann, M. Panchenko, and P. Zarka, editors, *Planetary Radio Emissions VIII*, pages 285–299, January 2017. doi: 10.1553/PRE8s285.

J. M. Grießmeier, A. Stadelmann, T. Penz, H. Lammer, F. Selsis, I. Ribas, E. F. Guinan, U. Motschmann, H. K. Biernat, and W. W. Weiss. The effect of tidal locking on the magnetospheric and atmospheric evolution of "Hot Jupiters". *Astronomy and Astrophysics*, 425:753–762, Oct 2004. doi: 10.1051/0004-6361:20035684.

J. M. Grießmeier, U. Motschmann, G. Mann, and H. O. Rucker. The influence of stellar wind conditions on the detectability of planetary radio emissions. *Astronomy and Astrophysics*, 437(2):717–726, Jul 2005. doi: 10.1051/0004-6361:20041976.

J. M. Grießmeier, P. Zarka, and H. Spreeuw. Predicting low-frequency radio fluxes of known extrasolar planets. *Astronomy and Astrophysics*, 475(1):359–368, Nov 2007. doi: 10.1051/0004-6361:20077397.

J. C. Guirado, R. Azulay, B. Gauza, M. A. Pérez-Torres, R. Rebolo, J. B. Climent, and M. R. Zapatero Osorio. Radio emission in ultracool dwarfs: The nearby substellar triple system VHS 1256-1257. *Astronomy and Astrophysics*, 610:A23, February 2018. doi: 10.1051/0004-6361/201732130.

Y. Gupta, B. Ajithkumar, H. S. Kale, S. Nayak, S. Sabhapathy, S. Sureshkumar, R. V. Swami, J. N. Chengalur, S. K. Ghosh, C. H. Ishwara-Chandra, B. C. Joshi, N. Kanekar, D. V. Lal, and S. Roy. The upgraded GMRT: opening new windows on the radio Universe. *Current Science*, 113(4):707–714, August 2017. doi: 10.18520/cs/v113/i04/707-714.

G. Hallinan, S. Bourke, C. Lane, A. Antonova, R. T. Zavala, W. F. Brisken, R. P. Boyle, F. J. Vrba, J. G. Doyle, and A. Golden. Periodic Bursts of Coherent Radio Emission from an Ultracool Dwarf. *Astrophysical Journal, Letters*, 663(1):L25–L28, July 2007. doi: 10.1086/519790.

G. Hallinan, A. Antonova, J. G. Doyle, S. Bourke, C. Lane, and A. Golden. Confirmation of the Electron Cyclotron Maser Instability as the Dominant Source of Radio Emission from Very Low Mass Stars and Brown Dwarfs. *Astrophysical Journal*, 684(1):644–653, September 2008. doi: 10.1086/590360.

G. Hallinan, S. K. Sirothia, A. Antonova, C. H. Ishwara-Chand ra, S. Bourke, J. G. Doyle, J. Hartman, and A. Golden. Looking for a Pulse: A Search for Rotationally Modulated Radio Emission from the Hot Jupiter, τ Boötis b. *Astrophysical Journal*, 762(1):34, Jan 2013. doi: 10.1088/0004-637X/762/1/34.

G. Hallinan, S. P. Littlefair, G. Cotter, S. Bourke, L. K. Harding, J. S. Pineda, R. P. Butler, A. Golden, G. Basri, J. G. Doyle, M. M. Kao, S. V. Berdyugina, A. Kuznetsov, M. P. Rupen, and A. Antonova. Magnetospherically driven optical and radio aurorae at the end of the stellar main sequence. *Nature*, 523(7562):568–571, July 2015. doi: 10.1038/nature14619.

Yasuhiro Hasegawa, Kazuhiro D. Kanagawa, and Neal J. Turner. Magnetic Fields and Accreting Giant Planets around PDS 70. *Astrophysical Journal*, 923(1):27, December 2021. doi: 10.3847/1538-4357/ac257b.

S. L. G. Hess and P. Zarka. Modeling the radio signature of the orbital parameters, rotation, and magnetic field of exoplanets. *Astronomy and Astrophysics*, 531:A29, July 2011. doi: 10.1051/0004-6361/201116510.

T. W. Hill. Inertial limit on corotation. *Journal of Geophysics Research*, 84(A11): 6554–6558, November 1979. doi: 10.1029/JA084iA11p06554.

T. W. Hill. The Jovian auroral oval. *Journal of Geophysics Research*, 106(A5):8101–8108, May 2001. doi: 10.1029/2000JA000302.

A. G. Hughes, A. C. Boley, R. A. Osten, J. A. White, and M. Leacock. Unlocking the Origins of Ultracool Dwarf Radio Emission. *Astronomical Journal*, 162(2):43, August 2021. doi: 10.3847/1538-3881/ac02c3.

Ruta Kale and C. H. Ishwara-Chandra. CAPTURE: a continuum imaging pipeline for the uGMRT. *Experimental Astronomy*, 51(1):95–108, February 2021. doi: 10.1007/s10686-020-09677-6.

Melodie M. Kao and J. Sebastian Pineda. Radio Emission from Binary Ultracool Dwarf Systems. *Astrophysical Journal*, 932(1):21, June 2022. doi: 10.3847/1538-4357/ac660b.

Melodie M. Kao, Gregg Hallinan, J. Sebastian Pineda, Ivanna Escala, Adam Burgasser, Stephen Bourke, and David Stevenson. Auroral Radio Emission from Late L and T Dwarfs: A New Constraint on Dynamo Theory in the Substellar Regime. *Astrophysical Journal*, 818(1):24, February 2016. doi: 10.3847/0004-637X/818/1/24.

Melodie M. Kao, Gregg Hallinan, J. Sebastian Pineda, David Stevenson, and Adam Burgasser. The Strongest Magnetic Fields on the Coolest Brown Dwarfs. *Astrophysical Journal, Supplement*, 237(2):25, August 2018. doi: 10.3847/1538-4365/aac2d5.

K. Katarzyński, M. Gawroński, and K. Goździewski. Search for exoplanets and brown dwarfs with VLBI. *Monthly Notices of the Royal Astronomical Society*, 461(1):929–938, September 2016. doi: 10.1093/mnras/stw1354.

S. Lacour, J. J. Wang, L. Rodet, M. Nowak, J. Shangguan, H. Beust, A. M. Lagrange, R. Abuter, A. Amorim, R. Asensio-Torres, M. Benisty, J. P. Berger, S. Blunt, A. Boccaletti, A. Bohn, M. L. Bolzer, M. Bonnefoy, H. Bonnet, G. Bourdarot, W. Brandner, F. Cantalloube, P. Caselli, B. Charnay, G. Chauvin, E. Choquet, V. Christiaens, Y. Clénet, V. Coudé Du Foresto, A. Cridland, R. Dembet, J. Dexter, P. T. de Zeeuw, A. Drescher, G. Duvert, A. Eckart, F. Eisenhauer, F. Gao, P. Garcia, R. Garcia Lopez, E. Gendron, R. Genzel, S. Gillessen, J. H. Girard, X. Haubois, G. Heißel, Th. Henning, S. Hinkley, S. Hippler, M. Horrobin, M. Houllé, Z. Hubert, L. Jocou, J. Kammerer, M. Keppler, P. Kervella, L. Kreidberg, V. Lapeyrère, J. B. Le Bouquin, P. Léna, D. Lutz, A. L. Maire, A. Mérand, P. Mollière, J. D. Monnier, D. Mouillet, E. Nasedkin, T. Ott, G. P. P. L. Otten, C. Paladini, T. Paumard, K. Perraut, G. Perrin, O. Pfuhl, E. Rickman, L. Pueyo, J. Rameau, G. Rousset, Z. Rustamkulov, M. Samland, T. Shimizu, D. Sing, J. Stadler, T. Stolker, O. Straub, C. Straubmeier, E. Sturm, L. J. Tacconi, E. F. van Dishoeck, A. Vigan, F. Vincent, S. D. von Fellenberg, K. Ward-Duong, F. Widmann, E. Wieprecht, E. Wiezorrek, J. Woillez, S. Yazici, A. Young, and Gravity Collaboration. The mass of β Pictoris c from β Pictoris b orbital motion. *Astronomy and Astrophysics*, 654:L2, October 2021. doi: 10.1051/0004-6361/202141889.

H. P. Ladreiter and Y. Leblanc. Jovian hectometric radiation - Beaming, source extension, and solar wind control. *Astronomy and Astrophysics*, 226(1):297–310, December 1989.

L. Lamy, P. Zarka, B. Cecconi, S. Hess, and R. Prangé. Modeling of Saturn kilometric radiation arcs and equatorial shadow zone. *Journal of Geophysical Research (Space Physics)*, 113(A10):A10213, October 2008. doi: 10.1029/2008JA013464.

Joseph Lazio, G. Hallinan, A. Airapetian, D. A. Brain, T. E. Clarke, T. Dolch, C. F. Dong, P. E. Driscoll, R. Fares, J. M. Griessmeier, W. M. Farrell, J. C. Kasper, T. Murphy, L. A. Rogers, E. Shkolnik, S. Stanley, A. Strugarek, N. J. Turner, A. Wolszczan, P. Zarka, M. Knapp, C. R. Lynch, and J. D. Turner. Magnetic Fields of Extrasolar Planets: Planetary Interiors and Habitability. *Bulletin of the American Astronomical Society*, 51(3):135, May 2019. doi: 10.48550/arXiv.1803.06487.

T. Joseph W. Lazio and W. M. Farrell. Magnetospheric Emissions from the Planet

Orbiting τ Bootis: A Multiepoch Search. *Astrophysical Journal*, 668(2):1182–1188, October 2007. doi: 10.1086/519730.

T. Joseph W. Lazio, S. Carmichael, J. Clark, E. Elkins, P. Gudmundsen, Z. Mott, M. Szwajkowski, and L. A. Hennig. A Blind Search for Magnetospheric Emissions from Planetary Companions to Nearby Solar-Type Stars. *Astronomical Journal*, 139(1):96–101, January 2010a. doi: 10.1088/0004-6256/139/1/96.

T. Joseph W. Lazio, P. D. Shankland, W. M. Farrell, and D. L. Blank. Radio Observations of HD 80606 Near Planetary Periastron. *Astronomical Journal*, 140(6):1929–1933, Dec 2010b. doi: 10.1088/0004-6256/140/6/1929.

W. Lazio, T. Joseph, W. M. Farrell, Jill Dietrick, Elizabeth Greenlees, Emily Hogan, Christopher Jones, and L. A. Hennig. The Radiometric Bode's Law and Extrasolar Planets. *Astrophysical Journal*, 612(1):511–518, Sep 2004. doi: 10.1086/422449.

A. Lecavelier Des Etangs, S. K. Sirothia, Gopal-Krishna, and P. Zarka. GMRT radio observations of the transiting extrasolar planet HD 189733 b at 244 and 614 MHz. *Astronomy and Astrophysics*, 500(3):L51–L54, June 2009. doi: 10.1051/0004-6361/200912347.

A. Lecavelier Des Etangs, S. K. Sirothia, Gopal-Krishna, and P. Zarka. GMRT search for 150 MHz radio emission from the transiting extrasolar planets HD 189733 b and HD 209458 b. *Astronomy and Astrophysics*, 533:A50, September 2011. doi: 10.1051/0004-6361/201117330.

A. Lecavelier des Etangs, S. K. Sirothia, Gopal-Krishna, and P. Zarka. Hint of 150 MHz radio emission from the Neptune-mass extrasolar transiting planet HAT-P-11b. *Astronomy and Astrophysics*, 552:A65, Apr 2013. doi: 10.1051/0004-6361/201219789.

Liming Li, X. Jiang, R. A. West, P. J. Gierasch, S. Perez-Hoyos, A. Sanchez-Lavega, L. N. Fletcher, J. J. Fortney, B. Knowles, C. C. Porco, K. H. Baines, P. M. Fry, A. Mallama, R. K. Achterberg, A. A. Simon, C. A. Nixon, G. S. Orton, U. A. Dyudina, S. P. Ewald, and R. W. Schmude. Less absorbed solar energy and more internal heat for Jupiter. *Nature Communications*, 9:3709, September 2018. doi: 10.1038/s41467-018-06107-2.

C. Lynch, T. Murphy, V. Ravi, G. Hobbs, K. Lo, and C. Ward. Radio detections of southern ultracool dwarfs. *Monthly Notices of the Royal Astronomical Society*, 457 (2):1224–1232, April 2016. doi: 10.1093/mnras/stw050.

C. R. Lynch, Tara Murphy, D. L. Kaplan, M. Ireland, and M. E. Bell. A search for circularly polarized emission from young exoplanets. *Monthly Notices of the Royal Astronomical Society*, 467(3):3447–3453, May 2017. doi: 10.1093/mnras/stx354.

C. R. Lynch, Tara Murphy, E. Lenc, and D. L. Kaplan. The detectability of radio emission from exoplanets. *Monthly Notices of the Royal Astronomical Society*, 478 (2):1763–1775, Aug 2018. doi: 10.1093/mnras/sty1138.

W. Majid, D. Winterhalter, I. Chandra, T. Kuiper, J. Lazio, C. Naudet, and P. Zarka. Search for Radio Emission from Extrasolar Planets: Preliminary Analysis of GMRT Data. In *Planetary Radio Emissions VI*, pages 589–594, January 2006.

Eric E. Mamajek and Cameron P. M. Bell. On the age of the β Pictoris moving group. *Monthly Notices of the Royal Astronomical Society*, 445(3):2169–2180, December 2014. doi: 10.1093/mnras/stu1894.

M. Mayor, M. Marmier, C. Lovis, S. Udry, D. Ségransan, F. Pepe, W. Benz, J. L. Bertaux, F. Bouchy, X. Dumusque, G. Lo Curto, C. Mordasini, D. Queloz, and N. C. Santos. The HARPS search for southern extra-solar planets XXXIV. Occurrence, mass distribution and orbital properties of super-Earths and Neptune-mass planets. *arXiv e-prints*, art. arXiv:1109.2497, Sep 2011.

M. McLean, E. Berger, J. Irwin, J. Forbrich, and A. Reiners. Periodic Radio Emission from the M7 Dwarf 2MASS J13142039+1320011: Implications for the Magnetic Field Topology. *Astrophysical Journal*, 741(1):27, November 2011. doi: 10.1088/

0004-637X/741/1/27.

M. McLean, E. Berger, and A. Reiners. The Radio Activity-Rotation Relation of Ultracool Dwarfs. *Astrophysical Journal*, 746(1):23, February 2012. doi: 10.1088/0004-637X/746/1/23.

Hitoshi Mizutani, Tetsuo Yamamoto, and Akio Fujimura. A new scaling law of the planetary magnetic fields. *Advances in Space Research*, 12(8):265–279, August 1992. doi: 10.1016/0273-1177(92)90397-G.

Przemek Mróz, Andrzej Udalski, Jan Skowron, Micha l K. Szymański, Igor Soszyński, Lukasz Wyrzykowski, Pawe l Pietrukowicz, Szymon Koz lowski, Rados law Poleski, Krzysztof Ulaczyk, Krzysztof Rybicki, and Patryk Iwanek. Microlensing Optical Depth and Event Rate toward the Galactic Bulge from 8 yr of OGLE-IV Observations. *Astrophysical Journal, Supplement*, 244(2):29, Oct 2019. doi: 10.3847/1538-4365/ab426b.

Tara Murphy, Martin E. Bell, David L. Kaplan, B. M. Gaensler, André R. Offringa, Emil Lenc, Natasha Hurley-Walker, G. Bernardi, J. D. Bowman, F. Briggs, R. J. Cappallo, B. E. Corey, A. A. Deshpand e, D. Emrich, R. Goeke, L. J. Greenhill, B. J. Hazelton, J. N. Hewitt, M. Johnston-Hollitt, J. C. Kasper, E. Kratzenberg, C. J. Lonsdale, M. J. Lynch, S. R. McWhirter, D. A. Mitchell, M. F. Morales, E. Morgan, D. Oberoi, S. M. Ord, T. Prabu, A. E. E. Rogers, D. A. Roshi, N. Udaya Shankar, K. S. Srivani, R. Subrahmanyan, S. J. Tingay, M. Waterson, R. B. Wayth, R. L. Webster, A. R. Whitney, A. Williams, and C. L. Williams. Limits on low-frequency radio emission from southern exoplanets with the Murchison Widefield Array. *Monthly Notices of the Royal Astronomical Society*, 446(3):2560–2565, Jan 2015. doi: 10.1093/mnras/stu2253.

Mayank Narang. The nature of the radio source detected towards the exoplanet system 1RXS1609.1-210524. *Monthly Notices of the Royal Astronomical Society*, 515(2):2015–2019, September 2022. doi: 10.1093/mnras/stac1902.

Mayank Narang, P. Manoj, and C. H. Ishwara Chandra. GMRT Observations of the Exoplanetary Systems τ Boötis and 55 Cancri. *Research Notes of the American Astronomical Society*, 5(7):158, July 2021a. doi: 10.3847/2515-5172/ac0fe0.

Mayank Narang, P. Manoj, C. H. Ishwara Chandra, Joseph Lazio, Thomas Henning, Motohide Tamura, Blesson Mathew, Nitish Ujwal, and Pritha Mandal. In search of radio emission from exoplanets: GMRT observations of the binary system HD 41004. *Monthly Notices of the Royal Astronomical Society*, 500(4):4818–4826, January 2021b. doi: 10.1093/mnras/staa3565.

Mayank Narang, Apurva V. Oza, Kaustubh Hakim, P. Manoj, Ravinder K. Banyal, and Daniel P. Thorngren. Radio-loud Exoplanet-exomoon Survey: GMRT Search for Electron Cyclotron Maser Emission. *Astronomical Journal*, 165(1):1, January 2023a. doi: 10.3847/1538-3881/ac9eb8.

Mayank Narang, Apurva V. Oza, Kaustubh Hakim, P. Manoj, Himanshu Tyagi, Bihan Banerjee, Arun Surya, Prasanta K. Nayak, Ravinder K. Banyal, and Daniel P. Thorngren. uGMRT observations of the hot-Saturn WASP-69b: Radio-Loud Exoplanet-Exomoon Survey II (RLEES II). *Monthly Notices of the Royal Astronomical Society*, 522(2):1662–1668, June 2023b. doi: 10.1093/mnras/stad1027.

J. D. Nichols. Magnetosphere-ionosphere coupling at Jupiter-like exoplanets with internal plasma sources: implications for detectability of auroral radio emissions. In *EPSC-DPS Joint Meeting 2011*, volume 2011, page 1353, October 2011.

J. D. Nichols. Candidates for detecting exoplanetary radio emissions generated by magnetosphere-ionosphere coupling. *Monthly Notices of the Royal Astronomical Society*, 427(1):L75–L79, November 2012. doi: 10.1111/j.1745-3933.2012.01348.x.

Eric L. Nielsen, Robert J. De Rosa, Jason J. Wang, Johannes Sahlmann, Paul Kalas, Gaspard Duchêne, Julien Rameau, Mark S. Marley, Didier Saumon, Bruce Macin-

tosh, Maxwell A. Millar-Blanchaer, Meiji M. Nguyen, S. Mark Ammons, Vanessa P. Bailey, Travis Barman, Joanna Bulger, Jeffrey Chilcote, Tara Cotten, Rene Doyon, Thomas M. Esposito, Michael P. Fitzgerald, Katherine B. Follette, Benjamin L. Gerard, Stephen J. Goodsell, James R. Graham, Alexandra Z. Greenbaum, Pascale Hibon, Li-Wei Hung, Patrick Ingraham, Quinn Konopacky, James E. Larkin, Jérôme Maire, Franck Marchis, Christian Marois, Stanimir Metchev, Rebecca Oppenheimer, David Palmer, Jennifer Patience, Marshall Perrin, Lisa Poyneer, Laurent Pueyo, Abhijith Rajan, Fredrik T. Rantakyrö, Jean-Baptiste Ruffio, Dmitry Savransky, Adam C. Schneider, Anand Sivaramakrishnan, Inseok Song, Remi Soummer, Sandrine Thomas, J. Kent Wallace, Kimberly Ward-Duong, Sloane Wiktorowicz, and Schuyler Wolff. The Gemini Planet Imager Exoplanet Survey: Dynamical Mass of the Exoplanet β Pictoris b from Combined Direct Imaging and Astrometry. *Astronomical Journal*, 159(2):71, February 2020. doi: 10.3847/1538-3881/ab5b92.

M. Nowak, S. Lacour, A. M. Lagrange, P. Rubini, J. Wang, T. Stolker, R. Abuter, A. Amorim, R. Asensio-Torres, M. Bauböck, M. Benisty, J. P. Berger, H. Beust, S. Blunt, A. Boccaletti, M. Bonnefoy, H. Bonnet, W. Brandner, F. Cantalloube, B. Charnay, E. Choquet, V. Christiaens, Y. Clénet, V. Coudé Du Foresto, A. Cridland, P. T. de Zeeuw, R. Dembet, J. Dexter, A. Drescher, G. Duvert, A. Eckart, F. Eisenhauer, F. Gao, P. Garcia, R. Garcia Lopez, T. Gardner, E. Gendron, R. Genzel, S. Gillessen, J. Girard, A. Grandjean, X. Haubois, G. Heißel, T. Henning, S. Hinkley, S. Hippler, M. Horrobin, M. Houllé, Z. Hubert, A. Jiménez-Rosales, L. Jocou, J. Kammerer, P. Kervella, M. Keppler, L. Kreidberg, M. Kulikauskas, V. Lapeyrère, J. B. Le Bouquin, P. Léna, A. Mérand, A. L. Maire, P. Mollière, J. D. Monnier, D. Mouillet, A. Müller, E. Nasedkin, T. Ott, G. Otten, T. Paumard, C. Paladini, K. Perraut, G. Perrin, L. Pueyo, O. Pfuhl, J. Rameau, L. Rodet, G. Rodríguez-Coira, G. Rousset, S. Scheithauer, J. Shangguan, J. Stadler, O. Straub, C. Straubmeier, E. Sturm, L. J. Tacconi, E. F. van Dishoeck, A. Vigan, F. Vincent, S. D. von Fellenberg, K. Ward-Duong, F. Widmann, E. Wieprecht, E. Wiezorrek, J. Woillez, and Gravity Collaboration. Direct confirmation of the radial-velocity planet β Pictoris c. *Astronomy and Astrophysics*, 642:L2, October 2020. doi: 10.1051/0004-6361/202039039.

J. P. Noyola, S. Satyal, and Z. E. Musielak. Detection of Exomoons through Observation of Radio Emissions. *Astrophysical Journal*, 791(1):25, August 2014. doi: 10.1088/0004-637X/791/1/25.

J. P. Noyola, S. Satyal, and Z. E. Musielak. On the Radio Detection of Multiple-exomoon Systems due to Plasma Torus Sharing. *Astrophysical Journal*, 821(2):97, April 2016. doi: 10.3847/0004-637X/821/2/97.

E. O'Gorman, C. P. Coughlan, W. Vlemmings, E. Varenius, S. Sirothia, T. P. Ray, and H. Olofsson. A search for radio emission from exoplanets around evolved stars. *Astronomy and Astrophysics*, 612:A52, Apr 2018. doi: 10.1051/0004-6361/201731965.

Rachel A. Osten, Suzanne L. Hawley, Timothy S. Bastian, and I. Neill Reid. The Radio Spectrum of TVLM 513-46546: Constraints on the Coronal Properties of a Late M Dwarf. *Astrophysical Journal*, 637(1):518–521, January 2006. doi: 10.1086/498345.

Rachel A. Osten, N. Phan-Bao, Suzanne L. Hawley, I. Neill Reid, and Roopesh Ojha. Steady and Transient Radio Emission from Ultracool Dwarfs. *Astrophysical Journal*, 700(2):1750–1758, August 2009. doi: 10.1088/0004-637X/700/2/1750.

M. Pérez-Torres, J. F. Gómez, J. L. Ortiz, P. Leto, G. Anglada, J. L. Gómez, E. Rodríguez, C. Trigilio, P. J. Amado, A. Alberdi, G. Anglada-Escudé, M. Osorio, G. Umana, Z. Berdiñas, M. J. López-González, N. Morales, C. Rodríguez-López, and J. Chibueze. Monitoring the radio emission of Proxima Centauri. *Astronomy and Astrophysics*, 645: A77, January 2021. doi: 10.1051/0004-6361/202039052.

Ngoc Phan-Bao, Rachel A. Osten, Jeremy Lim, Eduardo L. Martín, and Paul T. P. Ho. Discovery of Radio Emission from the Tight M8 Binary LP 349-25. *Astrophysical*

Journal, 658(1):553–556, March 2007. doi: 10.1086/511061.

J. Sebastian Pineda and Jackie Villadsen. Coherent radio bursts from known M-dwarf planet-host YZ Ceti. *Nature Astronomy*, 7:569–578, May 2023. doi: 10.1038/s41550-023-01914-0.

Sohrab Rahvar. Gravitational Microlensing Events as a Target for the SETI project. *Astrophysical Journal*, 828(1):19, Sep 2016. doi: 10.3847/0004-637X/828/1/19.

A. Reiners and U. R. Christensen. A magnetic field evolution scenario for brown dwarfs and giant planets. *Astronomy and Astrophysics*, 522:A13, November 2010. doi: 10.1051/0004-6361/201014251.

Tyler Richey-Yowell, Melodie M. Kao, J. Sebastian Pineda, Evgenya L. Shkolnik, and Gregg Hallinan. On the Correlation between L Dwarf Optical and Infrared Variability and Radio Aurorae. *Astrophysical Journal*, 903(1):74, November 2020. doi: 10.3847/1538-4357/abb826.

Matthew Route and Alexander Wolszczan. The Second Arecibo Search for 5 GHz Radio Flares from Ultracool Dwarfs. *Astrophysical Journal*, 830(2):85, October 2016. doi: 10.3847/0004-637X/830/2/85.

C. T. Russell. Re-evaluating Bode's law of planetary magnetism. *Nature*, 272(5649): 147–148, March 1978. doi: 10.1038/272147a0.

V. B. Ryabov, P. Zarka, and B. P. Ryabov. Search of exoplanetary radio signals in the presence of strong interference: enhancing sensitivity by data accumulation. *Planetary Space Science*, 52(15):1479–1491, December 2004. doi: 10.1016/j.pss.2004.09.019.

Sedighe Sajadian and Sohrab Rahvar. Illuminating hot Jupiters in caustic crossing. *Monthly Notices of the Royal Astronomical Society*, 407(1):373–380, Sep 2010. doi: 10.1111/j.1365-2966.2010.16901.x.

A. Sánchez-Lavega. The Magnetic Field in Giant Extrasolar Planets. *Astrophysical Journal, Letters*, 609(2):L87–L90, July 2004. doi: 10.1086/422840.

J. Sanz-Forcada, G. Micela, I. Ribas, A. M. T. Pollock, C. Eiroa, A. Velasco, E. Solano, and D. García-Álvarez. Estimation of the XUV radiation onto close planets and their evaporation. *Astronomy and Astrophysics*, 532:A6, August 2011. doi: 10.1051/0004-6361/201116594.

J. Saur, T. Grambusch, S. Duling, F. M. Neubauer, and S. Simon. Magnetic energy fluxes in sub-Alfvénic planet star and moon planet interactions. *Astronomy and Astrophysics*, 552:A119, April 2013. doi: 10.1051/0004-6361/201118179.

Y. Shiratori, H. Yokoo, T. Saso, O. Kameya, K. Iwadate, and K. Asari. Ten years of quests for radio bursts from extrasolar planets. In L. Arnold, F. Bouchy, and C. Moutou, editors, *Tenth Anniversary of 51 Peg-b: Status of and prospects for hot Jupiter studies*, pages 290–292, February 2006.

A. M. S. Smith, A. Collier Cameron, J. Greaves, M. Jardine, G. Langston, and D. Backer. Secondary radio eclipse of the transiting planet HD 189733 b: an upper limit at 307-347 MHz. *Monthly Notices of the Royal Astronomical Society*, 395(1):335–341, May 2009. doi: 10.1111/j.1365-2966.2009.14510.x.

Ignas A. G. Snellen, Bernhard R. Brandl, Remco J. de Kok, Matteo Brogi, Jayne Birkby, and Henriette Schwarz. Fast spin of the young extrasolar planet β Pictoris b. *Nature*, 509(7498):63–65, May 2014. doi: 10.1038/nature13253.

Ian R. Stevens. Magnetospheric radio emission from extrasolar giant planets: the role of the host stars. *Monthly Notices of the Royal Astronomical Society*, 356(3):1053–1063, January 2005. doi: 10.1111/j.1365-2966.2004.08528.x.

D. J. Stevenson. REVIEW ARTICLE: Planetary magnetic fields. *Reports on Progress in Physics*, 46(5):555–620, May 1983. doi: 10.1088/0034-4885/46/5/001.

A. Stroe, I. A. G. Snellen, and H. J. A. Röttgering. A stringent upper limit to 18 cm radio emission from the extrasolar planet system τ Boötis. *Astronomy and Astrophysics*, 546:A116, Oct 2012. doi: 10.1051/0004-6361/201220006.

N. Thomas, F. Bagenal, T. W. Hill, and J. K. Wilson. The Io neutral clouds and plasma torus. In Fran Bagenal, Timothy E. Dowling, and William B. McKinnon, editors, *Jupiter. The Planet, Satellites and Magnetosphere*, volume 1, pages 561–591. 2004.

Rudolf A Treumann. The electron–cyclotron maser for astrophysical application. *The Astronomy and Astrophysics Review*, 13(4):229–315, 2006.

J. D. Turner, J. M. Griessmeier, P. Zarka, and I. Vasylieva. The search for radio emission from exoplanets using LOFAR low-frequency beam-formed observations: Data pipeline and preliminary results for the 55 Cnc system. In G. Fischer, G. Mann, M. Panchenko, and P. Zarka, editors, *Planetary Radio Emissions VIII*, pages 301–313, January 2017. doi: 10.1553/PRE8s301.

Jake D. Turner, Philippe Zarka, Jean-Mathias Grießmeier, Joseph Lazio, Baptiste Cecconi, J. Emilio Enriquez, Julien N. Girard, Ray Jayawardhana, Laurent Lamy, Jonathan D. Nichols, and Imke de Pater. The search for radio emission from the exoplanetary systems 55 Cancri, υ Andromedae, and τ Boötis using LOFAR beam-formed observations. *Astronomy and Astrophysics*, 645:A59, January 2021. doi: 10.1051/0004-6361/201937201.

Sam Turnpenney, Jonathan D. Nichols, Graham A. Wynn, and Matthew R. Burleigh. Exoplanet-induced Radio Emission from M Dwarfs. *Astrophysical Journal*, 854(1): 72, February 2018. doi: 10.3847/1538-4357/aaa59c10.48550/arXiv.1801.01324.

H. K. Vedantham, J. R. Callingham, T. W. Shimwell, C. Tasse, B. J. S. Pope, M. Bedell, I. Snellen, P. Best, M. J. Hardcastle, M. Haverkorn, A. Mechev, S. P. O'Sullivan, H. J. A. Röttgering, and G. J. White. Coherent radio emission from a quiescent red dwarf indicative of star-planet interaction. *Nature Astronomy*, 4:577–583, February 2020. doi: 10.1038/s41550-020-1011-9.

H. K. Vedantham, Trent J. Dupuy, E. L. Evans, A. Sanghi, J. R. Callingham, T. W. Shimwell, W. M. J. Best, M. C. Liu, and P. Zarka. Polarised radio pulsations from a new T dwarf binary. *arXiv e-prints*, art. arXiv:2301.01003, January 2023. doi: 10.48550/arXiv.2301.01003.

C. Weber, H. Lammer, I. F. Shaikhislamov, J. M. Chadney, N. Erkaev, M. L. Khodachenko, J. M. Griessmeier, H. O. Rucker, C. Vocks, W. Macher, P. Odert, and K. G. Kislyakova. On the Cyclotron Maser Instability in Magnetospheres of Hot Jupiters - Influence of ionosphere models. In G. Fischer, G. Mann, M. Panchenko, and P. Zarka, editors, *Planetary Radio Emissions VIII*, pages 317–329, January 2017a. doi: 10.1553/PRE8s317.

C. Weber, H. Lammer, I. F. Shaikhislamov, J. M. Chadney, M. L. Khodachenko, J. M. Grießmeier, H. O. Rucker, C. Vocks, W. Macher, P. Odert, and K. G. Kislyakova. How expanded ionospheres of Hot Jupiters can prevent escape of radio emission generated by the cyclotron maser instability. *Monthly Notices of the Royal Astronomical Society*, 469(3):3505–3517, August 2017b. doi: 10.1093/mnras/stx1099.

C. Weber, N. V. Erkaev, V. A. Ivanov, P. Odert, J. M. Grießmeier, L. Fossati, H. Lammer, and H. O. Rucker. Supermassive hot Jupiters provide more favourable conditions for the generation of radio emission via the cyclotron maser instability - a case study based on Tau Bootis b. *Monthly Notices of the Royal Astronomical Society*, 480(3): 3680–3688, November 2018. doi: 10.1093/mnras/sty2079.

Peter K. G. Williams, Edo Berger, and B. Ashley Zauderer. Quasi-quiescent Radio Emission from the First Radio-emitting T Dwarf. *Astrophysical Journal, Letters*, 767 (2):L30, April 2013. doi: 10.1088/2041-8205/767/2/L30.

Robert M. Winglee, George A. Dulk, and Timothy S. Bastian. A Search for Cyclotron Maser Radiation from Substellar and Planet-like Companions of Nearby Stars. *Astrophysical Journal, Letters*, 309:L59, Oct 1986. doi: 10.1086/184760.

D. Winterhalter, T. Kuiper, W. Majid, I. Chandra, J. Lazio, P. Zarka, C. Naudet, G. Bryden, W. Gonzalez, and R. Treumann. Search for Radio Emissions from Extrasolar Planets:

the Observation Campaign. In *Planetary Radio Emissions VI*, pages 595–602, January 2006.

A. Wolszczan and D. A. Frail. A planetary system around the millisecond pulsar PSR1257 + 12. *Nature*, 355(6356):145–147, January 1992. doi: 10.1038/355145a0.

J. T. Wright, G. W. Marcy, A. W. Howard, John Asher Johnson, T. D. Morton, and D. A. Fischer. The Frequency of Hot Jupiters Orbiting nearby Solar-type Stars. *Astrophysical Journal*, 753(2):160, Jul 2012. doi: 10.1088/0004-637X/753/2/160.

CS Wu and LC Lee. A theory of the terrestrial kilometric radiation. *The Astrophysical Journal*, 230:621–626, 1979.

W. F. Yantis, III Sullivan, W. T., and W. C. Erickson. A Search for Extra-Solar Jovian Planets by Radio Techniques. In *Bulletin of the American Astronomical Society*, volume 9, page 453, June 1977.

P. Zarka. The Search for Exoplanetary Radio Emissions. In H. O. Rucker, W. S. Kurth, P. Louarn, and G. Fischer, editors, *Planetary, Solar and Heliospheric Radio Emissions (PRE VII)*, pages 287–301, January 2011.

P. Zarka, J. Queinnec, B. P. Ryabov, V. B. Ryabov, V. A. Shevchenko, A. V. Arkhipov, H. O. Rucker, L. Denis, A. Gerbault, P. Dierich, and C. Rosolen. Ground-Based High Sensitivity Radio Astronomy at Decameter Wavelengths. In *Planetary Radio Emission IV*, pages 101–127, Jan 1997.

P. Zarka, J. Lazio, and G. Hallinan. Magnetospheric Radio Emissions from Exoplanets with the SKA. In *Advancing Astrophysics with the Square Kilometre Array (AASKA14)*, page 120, April 2015.

Philippe Zarka. The auroral radio emissions from planetary magnetospheres: What do we know, what don't we know, what do we learn from them? *Advances in Space Research*, 12(8):99–115, Aug 1992. doi: 10.1016/0273-1177(92)90383-9.

Philippe Zarka. Auroral radio emissions at the outer planets: Observations and theories. *Journal of Geophysics Research*, 103(E9):20159–20194, September 1998. doi: 10.1029/98JE01323.

Philippe Zarka. Plasma interactions of exoplanets with their parent star and associated radio emissions. *Planetary Space Science*, 55(5):598–617, Apr 2007. doi: 10.1016/j.pss.2006.05.045.

Philippe Zarka, Rudolf A. Treumann, Boris P. Ryabov, and Vladimir B. Ryabov. Magnetically-Driven Planetary Radio Emissions and Application to Extrasolar Planets. *Astrophysics and Space Science*, 277:293–300, Jun 2001. doi: 10.1023/A:1012221527425.